Spatially offset Raman spectroscopy

Sara Mosca[1], Claudia Conti[2†], Nick Stone[3†], Pavel Matousek[1†]

[1]Central Laser Facility, STFC Rutherford Appleton Laboratory, Harwell Campus, Didcot, United Kingdom

[2]Consiglio Nazionale delle Ricerche, Istituto di Scienze del Patrimonio Culturale (ISPC), Milan, Italy

[3]School of Physics and Astronomy, University of Exeter, Exeter, United Kingdom

†Emails: Claudia Conti: claudia.conti@cnr.it, Nicholas Stone: N.Stone@exeter.ac.uk, Pavel Matousek: Pavel.Matousek@stfc.ac.uk

Author Contributions:

Introduction (N.S.), Experimentation (P.M., S.M.), Results (P.M., S.M.), Applications (C.C.), Reproducibility and data deposition (N.S.), Limitations and optimizations (P.M.), Outlook (N.S). Oversight of Primer (P.M.)

Abstract

Spatially offset Raman spectroscopy (SORS) is a spectroscopic technique that allows for the non-invasive chemical characterisation of diffusely scattering materials, ranging from opaque plastics to biological tissues. SORS has been explored for a range of applications, including disease diagnosis, the detection of explosives through unopened containers and the in-depth, non-destructive analysis of pharmaceutical products and objects of art. This Primer introduces the reader to the basic concepts underpinning SORS, details best practices for its implementation, highlights its use across multiple fields and provides insight into its limitations. The Primer concludes by discussing potential applications and envisaging future developments in the field.

[H1] Introduction

Spatially offset Raman spectroscopy (SORS) is a form of optical spectroscopy that allows the non-destructive, real-time analysis of the molecular composition of a sample. Similar to conventional Raman spectroscopy, the technique provides information on the chemical makeup of a sample by shining a laser on a sample and observing scattered photons of a different energy to the incident

35   photons[1]. In contrast to conventional Raman spectroscopy, SORS can probe deep inside diffusely

36   scattering objects such as tissue or powders and even probe through materials — for example, to

37   analyse the contents of an opaque plastic bottle. No sample preparation is required and the method

38   allows the sample to remain intact. Applications of SORS range from determining the chemical

39   composition of deep layers of paint on a work of art to the non-invasive monitoring of cancers[2] .

40

41   SORS and other Raman techniques rely on the detection of inelastically-scattered laser photons. The

42   majority of incident photons will cause an interacting molecule to instantaneously oscillate at the

43   same frequency as the incident photon before re-emitting another photon of identical energy in a

44   different direction — a process is known as Rayleigh scattering [G]. However, in cases where a

45   molecule has a fundamental vibrational mode at a much lower energy than the incident photon that

46   involves a change in the polarizability [G] of the molecule, then an inelastic or Raman scattering [G]

47   event can occur[1] **(Fig. 1),** which occurs once for every 10^6–10^8 elastic scattering events[3]. Raman

48   scattering typically results in the excitation of a molecule to a virtual energy level, followed by the

49   emission of a photon at the incident energy minus the energy donated to induce the molecular

50   vibration — a form of Raman scattering known as Stokes scattering. A photon incident on a

51   vibrationally-excited molecule can also gain energy and be emitted as a photon of a higher energy

52   than the incident photon. This process is known as anti-Stokes scattering and at room temperature

53   for higher vibrational modes is a relatively rare event[4]; for example, at 20 ^{o}C the anti-Stokes to Stokes

54   signal intensity ratios following excitation with an 830 nm laser are 0.64, 0.029 and 0.00086 for Raman

55   wavenumbers of 100 cm^{-1}, 800 cm^{-1} and 1600 cm^{-1}, respectively[5].

56

57   Raman spectroscopy identifies the molecular composition of a sample from specific shifts in photon

58   energy following Stokes or anti-Stokes scattering. Each photon spectral shift corresponds to the

59   frequency of a specific vibrational mode of the molecule. These Raman shifts can be measured in a

60   resultant Raman spectrum and serve as a 'molecular fingerprint' that enables the identification of

61   chemicals and materials. They can also identify dynamic changes — for example, molecular

62   conformational changes such as the rotation of a group of atoms within a molecule[6] — and reflect the

63   local environment of the molecule, such as the polarity of a solution or the presence or absence of

64   hydrogen bonds[7,8]. Molecular identification can be performed by comparing the measured Raman

65   spectra to those from standard samples stored in a library database. Raman shift is expressed in

66   relative wavenumbers (cm^{-1}) and is itself an expression of the difference between the absolute

67   wavenumber of the laser wavelength ($1/\lambda_L$) and the absolute wavenumber of the Raman emitted

68   photon ($1/\lambda_R$)[1]. The spectral region of the Raman spectra captured by a spectrograph is called the

69   spectral range and is typically 0–4000 cm^{-1}, where most vibrational modes lie, with signal detected at

70   a wavenumber of 0 cm^{-1} representing photons from the incident laser. Raman shift is directly

71   proportional to the energy change of photons upon Raman scattering and therefore independent of

72   excitation wavelength, making the comparison of acquired Raman spectra with those from reference

73   libraries straightforward.

74

75   Raman spectroscopy is complementary to infrared spectroscopy. Symmetric stretching vibrational

76   modes that alter the molecule polarizability tend to yield stronger Raman bands, whereas anti-

77   symmetric vibrations that alter the dipole moment of the molecule appear strong in infrared

78   absorption spectroscopy[9] **(Box 1)**. The techniques often have different application niches stemming

79   from the practicality of their deployment; for example, Raman inherently penetrates deep inside

80   materials, unlike equivalent infrared techniques that probe fundamental vibrational modes such as

81   mid-infrared spectroscopy[10]. Further, as the Raman signal of water is weak, it is better positioned for

82   probing deep inside living tissue compared to mid-infrared spectroscopy[11].

83

84   Conventional Raman studies generally use a backscattering setup, in which the illuminating laser and

85   detector for measuring the scattered Raman light partially follow the same optical path and target the

86   same area. With opaque samples, this approach is limited to surface observations as photon diffusion

87   in the sample results in the vast majority of the Raman photons originating from or near the surface[10].

88   Raman photons from deep into the material are not collected effectively as most are absorbed by the

89   material or spread sideways away from the collection area. Those few photons that originate from

90   deep in the sample and emerge at the collection area are often highly diluted by the photon diffusion

91   process and masked by near-surface originating Raman and fluorescence signals. Further, photon shot

92   noise **[G]** from signals originating from surface layers dwarfs those from deeper layers[12]. In biological

93   tissues, conventional Raman microscopy techniques are generally only effective at spatially resolving

94   signals from within 100–200 μm into the sample surface[10]. SORS allows for the rejection of surface

95   scattered photons through the use of spatially distinct illumination and collection regions, separated

96   by a spatial offset Δs[13]. Elastically-scattered and inelastically-scattered photons must travel laterally in

97   the sample to reach the spatially offset collection zone and detected photons therefore on average

98   emanate from deeper into the sample than in backscattering setups **(Fig. 2)**. A range of illumination–

99   collection offsets can allow for the collection of Raman signals from a range of depths.

100

101   In this Primer, we will provide an overview of the rapidly advancing field of SORS and its variants and

102   discuss the advantages and disadvantages of using SORS approach for various applications. The aim

103   of the Primer is to provide a springboard for those seeking to use this technique in their work, and to

104   provide appropriate instructions and references to enable the next steps to be taken by the reader.

105   We wish to note that in contrast with a conventional review, this Primer aims to cover key studies

106   exemplifying the technique and its applications rather than providing a comprehensive overview of

107   the work carried out in this area.

108

109   **[H1] Experimentation**

110

111   In this section we describe equipment and materials needed for experimental design, setting up

112   equipment, preparing samples and provide instructions on how to effectively collect SORS data.

113

114   [H2] Samples suitable for SORS

115   Although SORS shares many common properties with conventional Raman spectroscopy, its key

116   feature is its ability to probe through diffusely scattering materials, in which photons propagate in a

117   random-like fashion[13,14]. SORS is therefore useful for analyzing such materials where the inside or

118   subsurface is of interest rather than the top layer. The SORS technique is related to subsurface-probing

119   modalities previously used for near-infrared spectroscopy and fluorescence tomography in that it

120   involves light illumination and the detection of light that interacted with sample[15,16], although it offers

121   a higher degree of chemical specificity than these techniques. Diffusely scattering materials are

122   materials that we cannot see through or inside of clearly and are often referred to in the literature as

123   'turbid', or perhaps less accurately as 'translucent', 'non-transparent' or 'opaque'[17–20]. This is in

124   contrast with transparent samples (often referred to as 'clear') through which we can clearly visualise

125   objects. The majority of materials are diffusely scattering; examples include powders, milk, biological

126   tissues, layers of paint and opaque plastics. The propagation of laser and Raman photons through

127   diffusely scattering samples resembles a random walk, with photons changing their direction due to

128   light scattering and refraction and reflection at refractive index discontinuities within the sample.

129

130   Most diffusely scattering samples are suitable for SORS analysis; however, the sample should not be

131   excessively absorptive at laser and Raman excitation wavelengths to permit photon migration to and

132   from the layer of interest. The propagation of photons in the material can be characterized to

133   understand the extent of the SORS-probed zone using preliminary SORS experiments or using infrared

134   spatially-resolved and/or time-resolved approaches[21–26]. These methods can determine the photon

135   transport length, which describes the distance at which the photon direction is effectively fully

136   randomised — often through a number of individual scattering events where each one is somewhat

137   forward-biased — and infrared methods can also establish the absorption coefficient, which describes

138   the photon absorption properties of the propagation matrix[27,28]. Both these parameters are generally

139   wavelength dependent[29]. Although they describe the physics of the underlying photon diffusion

140   processes, the knowledge of these parameters is not absolutely required for basic SORS data analysis

141   aiming to recover pure Raman signatures of individual layers in a stratified sample.

142

143   [H2] A typical SORS instrument

144   A conventional SORS instrument comprises similar key components to a conventional Raman device

145   apart from the SORS signal readout being performed in a spatially offset manner (away from the laser

146   illumination area on the sample surface), preferably with variable spatial offset. The key components

147   of a SORS instrument are a laser source, an optical relay of laser light to the sample including spectral

148   purification filter(s) (bandpass or short pass filters, often termed 'laser line filters'), a sample holder,

149   a Raman spectrometer and an optical sensor — typically a charge-coupled device (CCD) camera **(Fig.**

150   **3a).** Laser light can be transferred from the laser to the sample using an optical relay system or using

151   an optical fibre; the latter conveniently mechanically decouples the laser from the sample area. The

152   laser line filter should be located after the fibre bundle as spurious Raman signal and fluorescence can

153   arise in the fibre, which then needs to be suppressed to visualise the weak Raman signals from the

154   sample[30]. The Raman spectrometer itself consists of an entrance slit, a lens collimating the light

155   emerging from the slit onto a dispersion grating and a lens focusing the spectrally dispersed light onto

156   an optical sensor **(Fig. 3b).** The Raman spectrometer can have an extra compartment on the input side

157   containing a long-pass or notch filter to spectrally filter Raman signal from the scattered laser

158   radiation. In cases where this extra filter stage is not included within the spectrometer, spectral

159   filtering must be performed by the user prior to coupling of detected light into the spectrometer.

160

161   SORS is often performed with high performance benchtop instruments; however, SORS instruments

162   can also be incorporated into much smaller, handheld devices[31]. Although handheld devices usually

163   have lower sensitivity and produce Raman spectra with a lower signal-to-noise ratio than desktop

164   instruments, they are often tailored to be adequate for an intended, specific application[31].

165

166   [H3] Laser and sensor properties

167   Laser light used for SORS must be spectrally narrow — ideally with a bandwidth of less than 1 cm^{-1} —

168   so as not to introduce unnecessary Raman line broadening. It must also be spectrally stabilized —

169   preferably to much less than ~1 cm^{-1} — in order not to induce undesirable spectral shifts to Raman

170   features during measurements. Often, near-infrared laser light is used to minimise interfering

171 fluorescence emission from the sample, which can interfere with detected Raman light and in severe
172 cases mask the Raman signal with associated photon shot noise and spectral distortions[32]. Although
173 fluorescence can originate from the target compound, in practice it frequently comes from sample
174 impurities[33,34]. Common SORS excitation wavelengths used are 785 nm, 808 nm and 830 nm; these
175 are used with the intention of generating a spectrum within the sensitive range of silicon based CCDs,
176 which extends up to around 1100 nm. Further fluorescence reduction can be achieved by using a near-
177 infrared (1064 nm) excitation laser; however, these necessitate the use of an indium gallium arsenide
178 (InGaAs) optical sensor, which typically have lower noise performance than CCDs. Further, this
179 excitation wavelength choice suffers from additional reduction in Raman yield compared with visible
180 laser excitation wavelengths owing to the dependence of Raman scattering probability[1] on $1/\lambda_L^4$. The
181 laser used for SORS experiments is typically a continuous-wave laser with an average power of several
182 hundred milliwatts, or tens of milliwatts for micro-SORS measurements. The dimensions of the
183 illuminated spot on the sample surface informs the laser intensity and is a key parameter determining
184 the threshold for sample damage, although it should be noted that this threshold is highly sample-
185 specific (discussed below)[35–37]. SORS devices intended for outside laboratory use are often in a light-
186 tight enclosure for safety and shielded from ambient light; where these are operated without such
187 enclosures the laser operator and bystanders may be required to wear laser eye protection and
188 operate the device under special safety protocols, for example the American National Standard
189 Z136.1-2014 ANSI and the International Standard IEC 60825:2020[38].

190

191 [H3] Collection system properties
192 Owing to the diffusion of photons in the sample and the natural wide-angle spread of Raman photons
193 emerging following Lambert's cosine law [G][39], the collection system needs to be capable of capturing
194 Raman light from a relatively large area at different spatial offsets — either sequentially or
195 simultaneously — and from the largest possible solid angle [G]. It must then convey this light
196 effectively to the spectrometer using either an open optical train or a fibre bundle, where it is imaged
197 onto its entrance slit within the acceptance angle [G] of the spectrometer. The collected light must be
198 spectrally filtered using long pass or notch filters before the spectrometer to separate elastically-
199 scattered and reflected laser light emerging from the sample from the useful Raman signal — in the
200 case of an optical fibre bundle, this is recommended to be performed before the light enters the
201 optical fibres to avoid laser light generating interfering fluorescence or Raman signal within the fibre
202 itself[40]. Two or three such filters used in series may be required in some circumstances to effectively
203 suppress intense laser radiation scattered from turbid samples.

204

205 Effective collection of Raman signal from an extended diffuse spot on the sample surface requires the

206 use of a spectrometer with a low f-number — typically 1.8, although an f-number of up to 3 could be

207 still be suitable — and a large slit height such as 6 or 8 mm[41]. The use of higher f-numbers or smaller

208 slit heights does not preclude SORS functionality but does reduce Raman collection efficiency. This can

209 be compensated for using longer acquisition times or higher laser powers. A spectroscopy-grade CCD

210 camera of at least 1024 pixels × 256 pixels is the most commonly used sensor in these applications.

211 CCDs with a greater pixel count can be used without compromising SORS performance; however, CCDs

212 of less than 1024 × 256 pixels are advised against as they can compromise spectral resolution, spectral

213 coverage and Raman collection efficiency. Typical SORS configurations are exemplified in references[42–

214 47].

215

216 [H2] Data collection

217 [H3] Sample considerations

218 The aim of SORS measurements is to acquire Raman spectra at one or more spatial offsets distributed

219 around the illumination zone to discern information on the subsurface composition of the sample.

220 Generally, no sample preparation is required for a SORS experiment; however, consideration needs to

221 be made for the sample to fit in front of the collection system and to ensure its chemical and physical

222 stability during measurements. Biological tissue may need to be wrapped in cling film or placed in an

223 environmental chamber for maintaining constant humidity to avoid drying during the measurement

224 [48,49].

225

226 [H3] Preventing and accounting for noise

227 The SORS instrument can exhibit thermal drift owing to small temperature fluctuations within the

228 spectrometer, which can impact relative wavenumbers[50] on the order of several cm^{-1}. The sensitivity

229 of the spectrometer to ambient temperature changes is typically minimised in the spectrometer

230 design and manufacturing stages, although residual sensitivity needs to be taken care of by stabilising

231 the external temperature. For measurements requiring a high degree of accuracy, the ambient

232 temperature should ideally be stabilised to within +/- 0.5^{o}C. This is often sufficient to provide a

233 spectrometer stability to well within 1 cm^{-1}. The sample and the collection system are typically

234 shielded from ambient light using an enclosure; if not available, placing a light-tight shroud over the

235 instrument sample area is sufficient. In a laboratory environment, lights can be turned off during

236 acquisition or the room can be illuminated using lights equipped with filters that block the

237 transmission of light in the spectral region where the Raman signal is detected. The environment

238 should be checked for remaining sources of light by carrying out a spectral acquisition with the laser

239 turned off. Light from computer monitors can cause undesirable background — particularly

240 problematic when monitoring weak Raman signals — and monitors can therefore also be equipped

241 with filters. Mobile phones should not be used during Raman acquisitions as light from the screen or

242 face scanning and photo range-finding emissions may also affect measurements.

243

244 Multiple acquisitions can be carried out at each spatial offset and averaged to enable effective removal

245 of cosmic rays [G] These are often removed by comparing multiply acquired spectra, a numerical

246 procedure which often requires three or more identical spectra to be collected sequentially[10].

247

248 Raman instruments need to be first calibrated so that the correct Raman shift in relative wavenumbers

249 (cm^{-1}) is rendered by the instrument. This is often performed by measuring a Raman standard with

250 known Raman wavenumber shifts and using a polynomial fit to provide a conversion from CCD pixels

251 to Raman wavenumbers (cm^{-1}). We refer readers to an ASTM E1840 guide on nominal Raman

252 frequencies of a range of common calibration standards[51,52].

253

254 The sample surface and the Raman signal should be monitored for the presence of any unexpected

255 changes that might be induced by excessive heating owing to laser illumination. Excessive heating can

256 damage the sample and potentially alter its chemical makeup. Such effects can be avoided by

257 decreasing the laser power, enlarging the laser illumination areas, rastering the laser beam across the

258 sample, or shortening the acquisition time [53,54].

259

260 [H3] Introducing spatial offsets

261 SORS spatial offsets are introduced by moving the laser beam across the sample surface (unless

262 multiple spatial offsets are collected simultaneously on the CCD sensor in the case of hyperspectral

263 SORS, discussed later). The magnitude of the spatial offset is often found by trial and error, optimising

264 the Raman signal-to-noise ratio from the target layer. Systematic investigations of the optimum spatial

265 offset for interrogating a specific depth have been carried out[47,55]. In general, to achieve similar signal-

266 to-noise ratio for all SORS spectra across a range of spatial offsets, longer acquisition times should be

267 used for larger spatial offsets as these usually yield weaker Raman signals.

268

269 Good practice when measuring signals from multiple spatial offsets or physically different sample

270 locations is repeat the first measurement after completion of all other measurements, so that one can

271 verify that no instrument misalignment, sample drift or other changes occurred over the course of the

272 experiment. When measuring more than two spatial offsets, it is also good practice to measure them

273   in a random order, rather than in an ascending or descending spatial offset order. This avoids the risk

274   of misinterpreting any instrumental drifts or gradual sample changes — induced by, for example,

275   photo-degradation or drying — by translating these into random data changes rather than systematic

276   error.

277

278   [H2] SORS variants

279   *[H3] Point-like SORS*

280   Similar to conventional Raman setups **(Fig 4A)**, the simplest SORS variant uses a point-like illumination

281   and collection geometry [13], although these are separated by the spatial offset in SORS **(Fig 4B)**. One or

282   more collection points can be imaged using a CCD camera; multiple collection points can be read

283   sequentially by moving the laser or collection area across the sample surface between acquisitions or

284   alternatively, data can be collected from multiple points simultaneously by collecting signal from each

285   spatial offset to a separate row on the CCD[40,45]. This technique — known as hyperspectral SORS — is

286   beneficial in situations where a sample is evolving in time, for example one undergoing a chemical

287   reaction or physically moving such as a live sample. However, different rows on the CCD yield slightly

288   different Raman spectral profiles and distortions caused by spectrograph imaging imperfections can

289   lead to artefacts in SORS processed data that then must be corrected numerically[43,56].

290

291   *[H3] Ring-collection SORS*

292   Ring-collection SORS uses a point-like illumination area, with Raman light collected using optical fibres

293   trained on the sample surface through a collection lens to form a collecting ring around the

294   illumination point. In this setup, the distance between the illumination area and the ringed collection

295   represents the specific spatial offset used **(Fig. 4C)**. Fibres can be organised in a complete ring[40] or just

296   a small segment[57], for example, to enable the use of a large number of spatial offsets simultaneously.

297   The collection fibres are arranged in a linear structure at the spectrograph entrance slit and brought

298   onto the spectrometer, enabling the simultaneous reading of different bundles (corresponding to

299   different spatial offsets) from separate rows of the CCD[40,58]. Another example of implementing the

300   ring-collection geometry includes using a digital micro-mirror device (DMD) arrangement, where a

301   programmable DMD is used to rapidly set a desired SORS spatial offset[59].

302

303   This ring-collection SORS geometry benefits from being able to average across larger sample areas

304   than point-like SORS, benefitting applications where laterally heterogeneous samples are probed and

305   averaged signals from the matrix are therefore required (for example, when deducing the average

306   composition of bone). In such applications, signals from different parts of the collection ring can be

307   summed. When high spatial resolution mapping of lateral heterogeneity is required, for example when

308   performing subsurface imaging to probe for hidden objects, individual parts of the ring can be read

309   separately.

310

311   *[H3] Ring-illumination SORS (inverse SORS)*

312   Raman signals can be read from a small area on the sample surface surrounded by a ring-shaped laser

313   illumination zone **(Fig. 4D)**[56,60]. This ring-illumination geometry is beneficial in applications where

314   sample damage must be avoided — for example, in *in vivo* applications or when examining precious

315   samples. Using this geometry, laser light can be spread over an increasingly wider area with increasing

316   spatial offsets, with higher laser powers used for larger spatial offsets where weaker signals are

317   present. This is advantageous in situations where maximum illumination intensity cannot be

318   exceeded, for example to avoid sample damage or to stay within safe illumination intensity limits

319   during in vivo applications. The same is not possible with conventional SORS using a ring or point-like

320   collection geometry.

321

322   *[H3] Defocusing SORS*

323   Defocusing SORS uses overlapping illumination and collection areas **(Fig. 4E)**. This variant is less

324   effective at providing contrast between the surface and subsurface layers than other modalities**;**

325   however, its key advantage is that it can be practised on conventional Raman systems without any

326   modifications. Defocusing SORS is performed by moving the sample away from the imaging position,

327   increasing both the laser illumination and Raman collection areas. In this process, although no actual

328   separation is achieved between the two areas, this leads to a SORS effect as the incidence of the laser

329   photon and the detection of the Raman photon can be spatially offset on the sample[61,62]. Defocusing

330   SORS results in the collection of spectra from a range of SORS offsets simultaneously, which enhances

331   depth sampling but does not suppress the surface signal to the same degree as other SORS modalities.

332

333   *[H3] Transmission Raman Spectroscopy*

334   Transmission Raman spectroscopy (TRS)[63,64] can be considered a special case of SORS where the

335   illumination and collection points are positioned on the opposite sides of a sample **(Fig. 4F)**. This is

336   only applicable for samples where both surfaces are accessible. Unlike other SORS modalities, TRS

337   does not enable the probing of individual layers in the sample – instead, it provides a volumetric signal,

338   approximating the average composition of the probed volume[63]. This can be beneficial in situations

339   where average volumetric sample composition is desirable, for example when quantifying

340   pharmaceutical formulations.

341

342   *[H3] Surface Enhanced Spatially Offset Raman Spectroscopy*

343   SORS can be combined with surface enhanced Raman spectroscopy (SERS) in a modality known as

344   SESORS[65,66]. SERS relies on the enhancement of Raman scattering by metal nanoparticles — often

345   made of gold or silver and typically approximately 80-200 nm in diameter — with their surface

346   plasmon resonance **[G]** (SPR) tuned to the laser excitation wavelength[67]. The large collective oscillation

347   of charge on the nanoparticle surface induced by light from the incident laser can lead to a 10^8–fold

348   boost of the Raman signal within several nanometres of the nanoparticle surface[68,69]; adding

349   nanoparticles to a sample can therefore dramatically boost SORS depth penetration, chemical

350   selectivity and sensitivity[66].

351

352   Modification of the nanoparticle surface can allow sensing of low-concentration analytes with high

353   chemical specificity;[70] for example, it is possible to analyse samples for the presence of antigens at low

354   concentrations using nanoparticles functionalised with antibodies, as antigen-antibody binding

355   induces subtle vibrational changes detectable through small Raman shifts of the tagged antibodies.

356   This approach can be used for disease diagnostic applications[71]. Further, the binding of nanoparticles

357   to single-stranded DNA can enable the monitoring of nucleic acids and their reactions[72]. A range of

358   other functionalisation options have been proposed and demonstrated (see ref[71]). Multiple different

359   nanoparticle surface attachments can be used simultaneously to allow for multiplexed monitoring of

360   chemical, physical and biological properties at depth[73,74].

361

362   *[H3] Micro-SORS*

363   In micro-SORS, laser light and collecting Raman signal are passed through a microscope objective and

364   the laser illumination spot, Raman collection area and spatial offset are on the scale of micrometres

365   to provide higher spatial resolution[75]. This modality is particularly advantageous when using highly

366   scattering samples or in cases where differentiation between layers is not possible with mm-scale

367   SORS — for example, when analysing layers of paint on a painting[75]. Two variations of micro-SORS

368   have been demonstrated to date: defocusing micro-SORS and full micro-SORS[76]. Defocusing micro-

369   SORS can be practised with a conventional Raman microscope[75] and is performed by moving the

370   sample from the imaged position away from the microscope objective rather than towards it to avoid

371   restrictions stemming from microscope objective working distance and the risk of touching the sample

372   with the microscope objective. Full micro-SORS[61] is performed by separating the laser illumination and

373   collection zones from each other, analogous to point-like SORS with much higher spatial resolution.

374   Full micro-SORS generally provides better layer contrast than defocusing micro-SORS and typically

375 requires modifications to be made to a standard Raman microscope instrument, such as: readjusting

376 the angle at which the laser beams enter the microscope objective[77]; using laser beam steering optics

377 within the microscope; bringing laser light to the sample using a separate, external microscope

378 objective[62] and modifying its data reading facility, for example by reading different zones on the

379 sample surface with different parts of the CCD sensor[78]. No special considerations apply to samples

380 for micro-SORS in general from those discussed above for SORS apart from the fact that samples need

381 to physically fit under the microscope objective of the Raman microscope. Because photon

382 propagation distances are shorter than those for SORS, the requirements for the absence of strong

383 absorption at the laser and Raman wavelengths are less stringent with micro-SORS. SORS variants are

384 compared directly in **Table 1.**

385

386 **[H1] Results**

387

388 In this section, we describe how SORS data is pre-processed and analysed to extract compositional

389 information on subsurface areas of sample.

390

391 [H2] Data pre-processing

392 Raw SORS spectra are typically pre-processed to remove background from fluorescence or ambient

393 light before analysis. The appearance of Raman band changes between spatial offsets indicates the

394 presence of more than one layer in the sample; if the relative Raman intensities are constant with the

395 spatial offset (and therefore imaging depth) then observed Raman bands likely to come from the same

396 chemical species, two different species are mixed up in a single layer, or multiple thin layers thinner

397 than the depth resolving power of the SORS variant used[79]. The rate of change of Raman band

398 intensities relative to each other also indicates the order of the layers[37]; the fastest decrease of

399 intensity as spatial offset increases is exhibited by the surface layer, then the second layer, then the

400 third and so forth. Each distinct sublayer induces a different rate of intensity change, informing the

401 number of detected layers. Caution should be exercised though when reaching conclusions based

402 solely on this information as other effects such as signal self-absorption in the matrix — which can

403 lead to distortions of relative Raman band intensities — can also contribute to these effects[42,80]. The

404 presence and magnitude of self-absorption can be deduced from the presence of changes of the

405 relative intensities of Raman bands belonging to a single chemical species. These are generally

406 invariant to spatial offset. For this, one requires the knowledge of the origin of individual Raman bands

407 and some Raman band assignment to individual molecular species would have to have been carried

408 out.

409

410 **[H2] Data analysis**

411 [H3] Differentiating layers

412 The first step of analysing SORS data is to retrieve the spectra of individual layers. For experiments

413 involving a two-layer system — for example, probing the contents of a container through the container

414 wall — the simplest approach relies on subtracting a zero-offset Raman spectrum (typically dominated

415 by surface layer contributions) from a SORS spectrum obtained at a non-zero spatial offset, which is a

416 representation of the subsurface layer. The non-zero offset spectrum can contain elements of the

417 surface layer Raman spectrum; therefore, an appropriate scaling factor chosen to cancel out any

418 contributions of the surface Raman spectra in the non-zero spatially offset spectrum is applied to the

419 subtracted, zero-offset spectrum **(Fig. 5)**[13]. The scaling factor is found commonly by trial and error

420 through observing the subtracted spectrum for the presence/absence of undesirable surface layer

421 Raman bands.

422

423 For a multilayer system with n layers where $n > 2$, one requires n spectra obtained at different spatial

424 offsets to retrieve Raman spectra from individual layers. The retrieval is analogous to the above

425 methodology where gradually a single layer Raman spectrum is cancelled in all the remaining spectra

426 until a pure Raman spectrum of the target layer is retrieved. Representative spectra illustrating the

427 separation of two layers from each other and associated mathematical steps are shown in **Fig.5**.

428 Currently, no commercially available software exists specifically for SORS data processing (apart from

429 those built into commercial SORS instruments[81,82]), although the above process can be accomplished

430 using Microsoft Excel[83] or Matlab[84], for example.

431

432 Differentiation of layers can also be performed using principal component analysis (PCA), which is

433 capable of separating the spectra according to variances present in the data sets[13]. This analysis

434 typically yields a linear combination of the Raman spectra of the layers, rather than the pure spectra

435 assignable directly to individual layers. For this to be effective, the number of spatially offset spectra

436 should ideally be an order of magnitude greater than the number of layers present[13]. To retrieve the

437 pure spectra of individual layers, additional mathematical processing must be performed. One method

438 for extracting pure Raman spectra of individual layers is band target entropy minimisation (BTEM),

439 which uses an algorithm that relies on the fact that, in general, a higher order exists in pure spectra

440 than those resulting from the summation of spectra from multiple layers[85]. A more advanced version

441 applicable to noisier data is adaptive-BTEM, which dynamically adapts convergence parameters during

442 the iterative search for real spectra[86]. An alternative effective approach for SORS spectral

443   decomposition is based on regression analysis, using the Raman spectra of known sample components

444   with the inclusion of regression residuals[87]. This is best used when the dominant chemical species of

445   the sample layers are known.

446

447   Many samples will have more complex stratification geometries than flat layers. For example, a

448   sample may contain a round object buried inside a matrix. Subject to yielding measurable signals,

449   these configurations can be analysed to retrieve estimates of pure spectra of individual chemically

450   distinct zones. Numerical methods such as Monte Carlo simulations **[G]** are often used to provide

451   further insight into the sample constitution or photon behaviour[88] and these are particularly useful

452   for complex geometries. Their validation is typically performed on test samples or imaging phantoms

453   **[G]** where stratification and constituency can be varied controllably[89]. Internal structural information

454   on chemically and physically distinct subsurface domains is generally required for the effective

455   deployment of Monte Carlo models. Photon trajectories calculated through Monte Carlo models

456   enable one to estimate the locations of laser photon-to-Raman photon conversion points in the matrix

457   for a given illumination and collection geometry, enabling the optimisation of these geometries

458   numerically by adjusting Monte Carlo parameters. This permits finding the optimum spatial offset,

459   laser and collection geometries for any given sample with a particular layer depth or an irregularly

460   shaped subsurface object in it and the deduction of the depths and lateral locations from which signals

461   originate.

462

463   [H3] Analyzing spectra

464   Once the spectra of individual layers are available, one can apply standard Raman analytical protocols

465   to retrieve the chemical and/or physical information contained within them. This can be carried out

466   by fitting individual Raman bands using Gaussian, Lorentzian or Voight shape-functions in software

467   such as Origin[90] or GRAMS/AI[91], using least squares methods, or using multivariate analysis methods

468   such as PCA, partial least squares (PLS) regression, multivariate curve resolution (MCR) or parallel

469   factor analysis (PARAFAC)[92], which can be achieved in Matlab[84] or SOLO[93].

470

471   Simple qualitative comparison of the observed Raman spectra with library Raman spectra [94–98] is often

472   used to identify chemical species; this can be performed by simple visual inspection, by using specialist

473   library search engines that often come with library packages (such as the Bruker OPUS software[99]) or

474   by performing a multivariate discriminant analysis (DA) — such as PCA-DA[92] — using software

475   packages such as Matlab[84] or SOLO[93]. SORS practitioners often build their own libraries containing the

476 common compounds that they analyse; alternatively, one can use molecular structure modelling

477 software capable of predicting Raman bands, such as the Gaussian software package[100].

478

479 The quantification of sample chemical subcomponents requires the building of a calibration spectra

480 set, which can be obtained from a set of samples with known concentration of subcomponents. As

481 Raman signal intensity scales linearly with sample concentration, the unknown concentration of

482 subcomponents in a sample can be determined using linear regression methods, for example using

483 the PLS method. This process is exemplified by the quantification of pharmaceutical formulations

484 using TRS in ref[101].

485

486 Measurements can be obtained from different spatial locations in order to derive chemical maps of

487 the sample surface. To analyse SORS maps, one should first extract the Raman signal of the target

488 layer from each individual location and then apply standard proprietary software used to analyse

489 conventional Raman maps such as Matlab[84], GRAMS/AI[91], WiRE[TM 102], Crytospec[103] or OPUS[99]. Analysis

490 of a sample at different time points or analysis of different samples can allow the tracking of dynamic

491 processes and sample-to-sample variations; in dynamic applications, one can ascertain sample

492 chemical composition both qualitatively and quantitatively as above.

493

494

495 **[H1] Applications**

496

497 Below, we discuss the wide range of SORS application areas developed over the recent years**.** The aim

498 of section is to exemplify the use of the SORS technique across multiple fields and does not represent

499 an exhaustive review of all SORS applications developed to date. Other application areas not covered

500 extensively in this section include those in the polymer sciences[104,105], petrochemical[106] and chemical

501 sciences[107] and manufacture[108], geology and mineralogy[109,110], biology[111] and manufacture and

502 cosmetics[112].

503

504 [H2] Pharmaceutical applications

505 SORS has a number of applications in the pharmaceutical field. Conventional SORS is well-suited to

506 the analysis of unopened pharmaceutical products for quality control purposes and to screen for

507 counterfeit drugs in sealed bottles and blister packs[113]. Typically, packaging of ~1–3 mm thickness can

508 be probed through, depending on the specific application[114]. This is also of interest to governmental

509 bodies overseeing safety of medical products or pharmaceutical companies and their distributors

510 ensuring the safety of their products. Further studies have shown the capability of SORS for
511 quantitative volumetric analysis of intact pharmaceutical tablets and capsules [64,115,116]. This application
512 has been developed commercially and SORS is now used by manufacturers to ensure that the
513 pharmaceutical formulations entering the market are within a permitted tolerance[117]. TRS specifically
514 is highly beneficial for this application as discussed in a recent review[118] as it overcomes subsampling
515 issues associated with conventional Raman spectroscopy, enabling it to provide a more representative
516 composition for often heterogeneous pharmaceutical products with thicknesses of up to ~ 10 mm.

517

518 Another major application of SORS is to confirm the composition of materials through unopened
519 packaging. Manufacturers of materials used for the production of active pharmaceutical ingredients
520 (API) are required by regulations to monitor that starting materials are correctly labelling before
521 distribution[119]. This can be performed by identifying the content of the packaged item chemically and
522 comparing it against its label; the process was until recently invasive and highly laborious, requiring
523 the opening of the packaging in a chemical sampling booth, material sampling and its subsequent
524 chemical analysis with techniques such as high performance liquid chromatography. Using SORS to
525 analyse the content of the packaging avoids the need to open the packaging and analysis can be
526 performed directly *in situ* with portable handheld SORS devices. In a proof-of-concept study, the
527 authors accurately identified common pharmaceutical materials through a number of commonly-used
528 packaging materials, including opaque plastic, paper sacks and coloured glass bottles, ensuring
529 analysis times as low as tens of seconds, operator safety and the integrity of inspected material. The
530 approach also eliminates the risk of cross-contamination and exposure to the ambient environment[55].
531 This application has also progressed to a commercial stage[120,121].

532

533 TRS can be used to quantify polymorphs [G] in a pharmaceutical formulation[122]. In a recent study, TRS
534 was shown to readily identify two polymorphs of flufenamic acid — a non-steroidal anti-inflammatory
535 drug —through their distinctly different Raman signatures. TRS was shown to be more accurate at
536 quantifying polymorphs than conventional Raman spectroscopy, owing to its volumetric sampling
537 capability and thus avoidance of subsampling issues caused by heterogeneous sample composition.
538 This is also now commercially[117]. Finally, a hyperspectral line mapping SORS configuration has been
539 used to monitor the thickness of the protective coatings of pharmaceutical tablets[123].

540

541 [H2] Security and forensics applications
542 SORS applications that have been developed and are widely used in the security field include the
543 scanning of medicines taken on board planes by passengers for essential medical reasons and the

544 scanning of duty-free items at airports for the presence of liquid and gel explosives[82,124]. SORS has the

545 potential to also detect toxic industrial chemicals, flammable compounds, explosives, narcotics and

546 chemical warfare agents at border checkpoints points and in emergency situations such as chemical

547 spillages, terrorist incidents and firefighting. Handheld SORS devices have been developed and are

548 used for these applications[125].

549

550 Another societally important application of SORS currently under development is the stand-off

551 detection of explosives through containers. Detection of explosives has been shown at distances of

552 over 10 m under ambient light conditions using time-resolved SORS[126,127]. The use of a near-infrared

553 excitation wavelength (1064 nm) minimizes interfering fluorescence, which may be present in

554 improvised explosive bottles owing to impurities[128].

555

556 The ability of SORS to detect the chemical composition of the contents of a turbid container was first

557 demonstrated in a study of bottles and jars common taken on board of plane by air passengers. The

558 study included containers with their original content and those containing a solution of 30% hydrogen

559 peroxide, which is a key component of a number of liquid explosives[124]. Although hydrogen peroxide

560 is a simple molecule with a low number of vibrational modes, it gives a distinct Raman signature,

561 enabling its clear identification. Other explosives typically yield much richer Raman spectra, further

562 aiding their identification[129,130]. For highly scattering containers such as those made of white plastic,

563 conventional Raman techniques were shown to detect only the signal originating from the container

564 wall; by contrast, SORS unequivocally identified the H_2O_2 marker band **(Fig. 6)**. Similar results have

565 been achieved with both transparent and other non-transparent container walls.

566

567 [H2] Medical applications

568 SORS has been investigated for the non-invasive sensing of the mineral and organic components of

569 bones to detect bone disorders[131], monitoring of bone regeneration[132] and screening for breast cancer

570 *in vivo*[41,133,134], with these applications currently in early development. SORS is well-suited to

571 examining bones as these are often located several millimetres below the skin surface and more easily

572 accessible from one side. TRS is a technique of choice for breast cancer screening as this organ is

573 accessible from two sides and TRS volumetric sensing is valuable when searching for the presence of

574 calcifications at unknown depths. TRS can probe samples of twice the thickness than the penetration

575 depth of conventional SORS[135]. SORS is also being investigated for the assessment of cancer margins

576 during breast cancer surgery in order to minimize the removal of normal tissue for medical and

577 aesthetic reasons[44,136]. The current approach is based on histopathological assessment of biopsied

578   tissue, often whilst the patient is still in surgery. Further applications have also been proposed based

579   on the ability of SORS to form 3D images of objects located deep inside a diffusely scattering matrix,

580   including those based on Raman tomographic imaging and image-guided Raman spectroscopy using

581   X-ray computed tomography for the diagnosis of bone disorders[137–143].

582

583   SORS and SESORS allow monitoring of the subsurface physical-chemical properties of tissues such as

584   temperature and pH[135]. This could allow for their use in subsurface monitoring of chemical or catalytic

585   processes[73,144]. SESORS has also been investigated for use in photo-thermal therapy with temperature

586   feedback[144,145]. A proof-of-concept study demonstrated the viability of heating of gold nanoparticles

587   embedded 5 mm deep in tissue by ~20 $^\circ$C by exciting these with a laser light and also showed

588   simultaneous non-invasive monitoring of tissue temperature at the same depth using a different set

589   of gold nanoparticles functionalised with temperature-reporting molecules[145].

590

591   Micro-SORS is being developed for the monitoring of blood quality as it allows the analysis of blood

592   quality in blood bags without opening the bags and potentially compromising sterility[77]. The decay

593   rate of blood varies enormously and consequently blood bags are discarded according to stringent

594   guidelines, potentially wasting good-quality blood; this could be prevented by through-bag blood

595   quality monitoring[77,146,147].

596

597   Recently, the detection of cancer lesions *in vivo* has been demonstrated by using nanoparticles with a

598   Raman reporter (IR 792 dye) functionalized with a cancer-targeting agent (cyclic-RGDyK peptide)

599   injected into mice and performing measurements through the mice skulls to generate SESORS maps[148].

600   The results were compared with those obtained using conventional Raman mapping, which was

601   unable to clearly delineate the lesion noninvasively.

602

603   Other medical applications for SORS that have been investigated so far include non-invasive glucose

604   detection[149] and low-level bioanalyte detection in brain tissue using SESORS[150]. An illustrative case

605   study in this field is the application of SESORS for the through-skull analysis of an agarose gel

606   containing varying concentrations of neurotransmitters and gold nanoparticles, where agarose gel

607   was used to mimic brain tissue [150–152]. The limits of detection for all studied neurotransmitters were

608   between 100 nM and 1 µM and corresponded to physiologically relevant concentrations[152]. **Fig. 7**

609   shows illustrative SESORS spectra from mixtures of neurotransmitters in agarose, collected through

610   an animal skull with 0 mm and 2 mm spatial offsets[152]**.** This study demonstrated the potential of

611   SESORS for non-invasive *in vivo* monitoring of neurotransmitter concentrations[151]; the ultimate goal

612   of this research area is the non-invasive diagnosis of neurological disorders such as Parkinson's and

613   Alzheimer's diseases at an early clinical stage[152].

614

615   [H2] Food sciences

616   SORS can be used to analyse the chemical composition of foodstuffs, for example to quantify the

617   lycopene content of intact tomatoes to monitor their ripening[153]. Hyperspectral SORS has been used

618   for the determination of the nutrient content and origin of potatoes[154] and the monitoring of carotene

619   content and iodine levels of intact salmon through the skin[35].

620

621   SORS can be used to detect adulterants in spirit beverages through bottles to identify counterfeit

622   products. In a proof-of-concept study, ten denaturant and flavouring additives were detected through

623   bottles at concentrations of approximately 1–100 ppm. SORS was shown to discriminate between

624   different Scotch whisky brands, allowing the identification of counterfeit products through

625   comparison with genuine product[155]. Counterfeiters often use genuine packaging and can closely

626   simulate genuine products; consequently, a highly sensitive and accurate method such as SORS is

627   required to differentiate between real and close copies of the product. The additives in the above

628   study were detected with a handheld SORS device[81], demonstrating the potential for *in situ* analysis

629   outside the laboratory environment. SORS could be extended to identify other counterfeit food

630   products.

631

632   [H2] Analysis of historical objects

633   Micro-SORS devices have been investigated for the analysis of the composition of paintings and

634   decorated objects, decay products located below the surface of these objects and the diffusion of

635   conservation treatments[156,157]. This knowledge is important as information on the subsurface chemical

636   makeup of these items enables better definition of condition, which is essential for applying

637   appropriate conservation treatments and avoiding the risk of any undue damage. Analysis is also

638   relevant to art history as it informs on the materials used by the artist, the artist's technique[158] and

639   the presence of signs or letters obscured by turbid materials such as paper[159]. Portable micro-SORS

640   devices enable investigations *in situ*, which is advantageous when sampling fragments or where

641   transfer of the object to the laboratory is unfeasible[160]. Recently, a portable micro-SORS device was

642   developed[161] and used for the reconstruction of the layer sequences of two 16th century panel

643   paintings *in situ*, providing information on the pigments used and the artist's technique[162]. Such

644   applications require care to avoid any undue damage from the laser beam and often very low laser

645   powers are used [163]. To avoid damage when carrying out such sensitive applications, one can use a

646   short acquisition time (for example, 0.1 ms) and carefully increase laser power, while observing the

647   sample using a portable optical microscope and simultaneously reading Raman spectra to look for any

648   initial signs of undue changes, such as spectral backgrounds rising faster than the Raman spectrum.

649   Using defocusing micro-SORS decreases laser intensity as offset increases and therefore its use could

650   offer further protection in some cases.

651

652   **[H1] Reproducibility and data deposition**

653

654   Different applications require different levels of data reproducibility; identification of chemicals, for

655   example, requires a lower level of accuracy compared to quantification applications. The

656   reproducibility of SORS data can be affected by multiple factors, including the spectrometer

657   calibration accuracy, its temperature and mechanical stability, laser frequency accuracy and stability.

658   CCD etaloning **[G]**, read-out noise **[G]** and thermal noise **[G]**, which are imprinted on spectral profiles,

659   can also affect subsequent spectral analysis results. Effects such as etaloning and spectrometer

660   calibration accuracy manifest themselves in SORS spectra as fixed distortions, whereas other effects

661   (for example laser frequency drift and spectrometer calibration drift) produce temporally evolving

662   spectral distortions that can negatively impact SORS measurements[50,56]. Fixed distortions become

663   important when transferring data between instruments as these can vary between different devices

664   and lead to distinct spectral profiles and systematic spectral shifts. As such, extra care needs to be

665   taken in situations where SORS spectra such as library spectra, or calibration spectra, are interchanged

666   between different instruments. Generally, SORS instruments are designed to minimise spectral

667   distortions and temporal drifts; for example, spectrographs are designed to avoid thermally-induced

668   or mechanically-induced motions that could lead to spectral drifts. The laser unit itself is often

669   thermally stabilized to avoid any frequency drifts. Furthermore, the utilisation of the source of a

670   known broadband spectral intensity profile — such as that produced by a fluorescence source or

671   emission lamp — can allow for a direct measurement of the instrument response function **[G]**, which

672   enables between-instrument differences to be corrected[164,165].

673

674   SORS data can be stored in numerous formats and generally, at present, there is no prescribed format

675   that should be used. Many vendors use their own proprietary data compression software and data

676   storage methods. For that reason, publicly presented data are often available in ASCII or MS Excel.csv

677   formats. Data files typically include Raman wavenumbers and Raman intensities for different SORS

678   spatial offsets. Metadata should include experimental conditions and sample information; for

679   example, chemical composition of the sample, physical state (temperature, layer thickness, solid or

680 liquid, crystalline form, polymorphic state, amorphous form), temperature and previous storage

681 conditions. Data on experimental parameters should include the total acquisition time, excitation

682 wavelength, laser power at the sample, dimensions of the collection and illumination areas, the spatial

683 offset used and the spectrograph spectral resolution. Information on the calibration method, whether

684 any cosmic ray removal was present and if any pre-processing was carried out on the recorded data

685 should also be given. Raw or minimally-processed data should be stored to ensure the highest possible

686 fidelity and flexibility in applying a pre-processing method of choice later. The data file can also contain

687 a readout with no laser radiation present, for the provision of ambient background indicating if any

688 significant spurious signals were present. Currently, no public SORS data repositories exist and SORS

689 practitioners also often develop their own libraries; however, Raman spectra can be looked up or

690 deposited in public depositories such as the Royal Society of Chemistry's ChemSpider[166] database. It

691 would be of great benefit to the spectroscopic community if SORS data could be shared in a similar

692 format in future. Specific libraries could be useful tools in application areas such as product

693 provenance; for example, identifying counterfeit drugs or adulterated food products.

694

695 **[H1] Limitations and optimizations**

696

697 There are a number of limitations that can restrict the deployment of SORS. The first one stems from

698 the inherent susceptibility of Raman spectroscopy to fluorescence, which is capable of creating large

699 backgrounds and potentially swamping Raman signal with photon shot noise. Such signals can

700 originate from the dominant components of a sample or sample impurities. This is particularly

701 problematic in situations where fluorescence emission occurs from a sample layer of interest. If the

702 fluorescence predominantly originates from a shallower layer than that of interest, it can be

703 suppressed by increasing spatial offset. The use of a near-infrared excitation wavelength can also

704 suppress fluorescence by minimising the likelihood of exciting the electronic states of molecules

705 within the sample. More complex schemes for avoiding fluorescence background have been

706 developed, including the temporal rejection of fluorescence[167–169]. This approach relies on the

707 difference in the temporal properties of fluorescence and Raman emission; as there is a delay between

708 excitation and fluorescence emissions corresponding to the fluorescence lifetime and Raman

709 scattering is instantaneous, the impulsive excitation of a Raman signal using picosecond laser pulses

710 and synchronous gated detection using a gated detector can allow the effective separation of Raman

711 scattered light from fluorescence signals.

712

713   SORS is limited in situations where the probed medium is highly absorptive at the laser or Raman

714   wavelength, which can lead to a severe reduction of photon propagation distances and a reduction in

715   the achievable penetration depth and sensitivity[170]. Absorption can be caused by electronic absorption

716   or near-infrared absorption – the former potentially being most severe[29]. Most SORS experiments are

717   performed using a near-infrared laser excitation wavelength to minimise absorption by the sample

718   constituents and suppress fluorescence.

719

720   The use of excessively high laser intensities can induce undesirable sample damage[171] or be in excess

721   of safety limits in *in vivo* application. This can be mitigated by expanding the laser illumination area on

722   the sample surface or reducing the laser power and extending the acquisition time. Some care has to

723   be taken when expanding the illumination area as an overly large sample illumination spot or Raman

724   collection zone in proportion to the spatial offset used leads to the reduction of SORS contrast

725   between different layers. Inverse SORS, which uses a ring illumination strategy, is well-suited for

726   photo-sensitive or thermally-sensitive samples as it can spread laser photons over a large area without

727   compromising layer contrast.

728

729   An additional SORS limitation is associated with the detection camera. A limited quantum efficiency

730   or elevated levels of thermal noise or readout noise can reduce the sensitivity or effective penetration

731   depth of SORS measurements. High-end spectroscopic CCD cameras reach levels of performance

732   where these limitations are negligible. These effects can, however, be significant with lower-cost,

733   lower performance CCDs often used in handheld devices for their lower footprint, weight,

734   consumption and cost.

735

736   Sample compositional heterogeneity can complicate the interpretation of SORS data — especially in

737   the case of micro-SORS where spatial resolution is high. In this case, variation of spatial offset can lead

738   to the crossing over from probing one heterogeneous domain to another, leading to lateral effects

739   being potentially attributed to spectral variations at different depths and complicating SORS data

740   analysis and interpretation. This can be mitigated by repeating the SORS measurements at multiple

741   locations on the sample surface and averaging the acquired signals or sampling with lower spatial

742   resolution instruments[172,173].

743

744   The commercial use of SORS is limited by the relatively high cost of the underpinning technology

745   (instrument costs tend to be greater than $10,000 USD). However, the cost of SORS devices is

746   expected to reduce considerably in the coming decade as the manufacture of components such as

747 lasers, filters, spectrographs and detectors increases to support the growth Raman spectroscopy in

748 general. The adoption of advanced complementary metal-oxide-semiconductor (CMOS) technology

749 for Raman spectroscopy to replace CCD sensors in SORS instruments may also take place[174]; these

750 components have already benefitted from volume cost reduction because of their implementation in

751 mobile phones.

752

753 **[H1] Outlook**

754

755 The non-destructive and non-invasive nature of SORS analysis allows for a range of applications, and

756 many more applications are likely to arise in the near future. Advances in the medical sector may

757 enable the continuous monitoring of medical conditions by using nanoparticles able to provide

758 condition specific signals available for direct SESORS readout[149]. Several pharmaceutical, forensics and

759 security applications have already made it to a commercial stage[175], with many others in

760 development[31]. The further development of SORS instrument components is expected to lead to

761 further miniaturisation of Raman spectrometers, which are expected to make the technology

762 implementable into mobile phones or even smaller devices[174,176,177]. The development of miniature

763 spectrometers based around interferometric detection is a promising area as it holds prospects for

764 mm-scale Raman spectrometers[178]. These technological advances are expected to open a host of

765 untapped markets, and allow the use of Raman outside of research laboratories. Improvements in

766 automated data processing are further likely to drive applications into new areas where non-

767 specialists are required to use devices; this process is already happening in the pharmaceutical and

768 security sectors but is expected in other fields[179,180]. The abovementioned advances in underpinning

769 SORS technology and data processing are likely to lead to improved sensitivity and depth probing,

770 which will likely impact on many applications too. A major beneficiary area is expected to be disease

771 diagnosis and monitoring, which is expected to benefit particularly strongly from these advances. It is

772 difficult to assess the impact of SORS technology further ahead, but it is certain that once

773 technological, cost and applications specific issues are addressed, the impact of SORS is likely to grow

774 and provide great benefits in many areas.

775

776 **References**

777 1.   Pelletier, M. J. *Analytical Applications of Raman Spectroscopy*. *Blackwell Science, Oxford* (1999).

778 2.   Matousek, P. Spatially offset Raman spectroscopy for non-invasive analysis of turbid samples. *TrAC*

779   *Trends Anal. Chem.* **103**, 209–214 (2018).

780 3.   Long, D. A. *The Raman Effect*. *The Raman effect: a unified treatment of the theory of Raman scattering*

781   *by molecules.* (John Wiley & Sons, Ltd, 2002). doi:10.1002/0470845767.

782   4.   Jones, R. R., Hooper, D. C., Zhang, L., Wolverson, D. & Valev, V. K. Raman Techniques: Fundamentals
783   and Frontiers. *Nanoscale Res. Lett.* **14**, 231 (2019).

784   5.   Tuschel, D. Raman thermometry. *Spectrosc. (Santa Monica)* **31**, 8–13 (2016).

785   6.   Iwata, K., Ozawa, R. & Hamaguchi, H. Analysis of the Solvent- and Temperature-Dependent Raman
786   Spectral Changes of S 1 trans -Stilbene and the Mechanism of the trans to cis Isomerization: Dynamic
787   Polarization Model of Vibrational Dephasing and the CC Double-Bond Rotation 7†. *J. Phys. Chem. A*
788   **106**, 3614–3620 (2002).

789   7.   Singh, A., Gangopadhyay, D., Nandi, R., Sharma, P. & Singh, R. K. Raman signatures of strong and weak
790   hydrogen bonds in binary mixtures of phenol with acetonitrile, benzene and orthodichlorobenzene. *J.*
791   *Raman Spectrosc.* **47**, 712–719 (2016).

792   8.   Wang, H. *et al.* Effects of hydrogen bond and solvent polarity on the C=O stretching of bis(2-
793   thienyl)ketone in solution. *J. Chem. Phys.* **136**, 124509 (2012).

794   9.   Hashimoto, K., Badarla, V. R., Kawai, A. & Ideguchi, T. Complementary vibrational spectroscopy. *Nat.*
795   *Commun.* **10**, 4411 (2019).

796   10.   Matousek, P. & Morris, M. D. *Emerging Raman Applications and Techniques in Biomedical and*
797   *Pharmaceutical Fields*. (Springer Berlin Heidelberg, 2010). doi:10.1007/978-3-642-02649-2.

798   11.   Nicolson, F., Kircher, M. F., Stone, N. & Matousek, P. Spatially offset Raman spectroscopy for
799   biomedical applications. *Chem. Soc. Rev.* **50**, 556–568 (2021).

800   12.   Matousek, P. Deep non-invasive Raman spectroscopy of living tissue and powders. *Chem. Soc. Rev.* **36**,
801   1292 (2007).

802   13.   Matousek, P. *et al.* Subsurface Probing in Diffusely Scattering Media Using Spatially Offset Raman
803   Spectroscopy. *Appl. Spectrosc.* **59**, 393–400 (2005). **The first conceptual demonstration of spatially**
804   **offset Raman spectroscopy (SORS).**

805   14.   Martelli, F., Bianco, S. del, Ismaelli, A. & Zaccanti, G. Photon Migration Through Diffusive Media:
806   Theory, Solutions, and Software. *Spie B.* 1365 (2009).

807   15.   Pfefer, T. J., Schomacker, K. T., Ediger, M. N. & Nishioka, N. S. Multiple-fiber probe design for
808   fluorescence spectroscopy in tissue. *Appl. Opt.* **41**, 4712 (2002).

809   16.   Shi, L. & Alfano, R. *Deep Imaging in Tissue and Biomedical Materials (Pan Stanford Publishing Pte*. (Ltd,
810   2017).

811   17.   Iping Petterson, I. E., Esmonde-White, F. W. L., de Wilde, W., Morris, M. D. & Ariese, F. Tissue
812   phantoms to compare spatial and temporal offset modes of deep Raman spectroscopy. *Analyst* **140**,
813   2504–2512 (2015).

814   18.   Gardner, B., Matousek, P. & Stone, N. Temperature Spatially Offset Raman Spectroscopy (T-SORS):
815   Subsurface Chemically Specific Measurement of Temperature in Turbid Media Using Anti-Stokes
816   Spatially Offset Raman Spectroscopy. *Anal. Chem.* **88**, 832–837 (2016).

817   19.   Everall, N. *et al.* Measurement of Spatial Resolution and Sensitivity in Transmission and Backscattering
818   Raman Spectroscopy of Opaque Samples: Impact on Pharmaceutical Quality Control and Raman
819   Tomography. *Appl. Spectrosc.* **64**, 476–484 (2010).

820 20. Oelkrug, D., Ostertag, E. & Kessler, R. W. Quantitative Raman spectroscopy in turbid matter: reflection
821   or transmission mode? *Anal. Bioanal. Chem.* **405**, 3367–3379 (2013).

822 21. Zaccanti, G., Del Bianco, S. & Martelli, F. Measurements of optical properties of high-density media.
823   *Appl. Opt.* **42**, 4023 (2003).

824 22. Pogue, brian w & Patterson, M. S. Frequency-domain optical absorption spectroscopy of finite tissue
825   volumes using diffusion theory tissue volumes using diffusion theory. *Phys. Med. Biol* **39**, 1157–1180
826   (1994).

827 23. Spinelli, L. *et al.* Calibration of scattering and absorption properties of a liquid diffusive medium at NIR
828   wavelengths. Time-resolved method. *Opt. Express* **15**, 6589 (2007).

829 24. Bouchard, J.-P. *et al.* Reference optical phantoms for diffuse optical spectroscopy Part 1 – Error
830   analysis of a time resolved transmittance characterization method. *Opt. Express* **18**, 11495 (2010).

831 25. Patterson, M. S., Chance, B. & Wilson, B. C. Time resolved reflectance and transmittance for the non-
832   invasive measurement of tissue optical properties. *Appl. Opt.* **28**, 2331–2336 (1989).

833 26. Mosca, S. *et al.* Estimating the Reduced Scattering Coefficient of Turbid Media using Spatially Offset
834   Raman Spectroscopy. *Anal. Chem.* In press (2021) **doi:10.1021/acs.analchem.0c04290.**

835 27. Das, B. B., Liu, F., R R Alfano & Alfano, R. R. Time-resolved fluorescence and photon migration studies
836   in biomedical and model random media,. *Rep. Prog. Phys* **60**, 227 (1997).

837 28. Brenan, C. J. H. & Hunter, I. W. Volumetric Raman Microscopy Through a Turbid Medium. *J. Raman
838   Spectrosc.* **27**, 561–570 (1996).

839 29. Mosca, S. al. Optical characterisation of porcine tissues from various organs in the 650 -- 1100 nm
840   range using time-domain diffuse spectroscopy. *BOE Opt* **11**, 1697–1706 (2020).

841 30. Stevens, O., Iping Petterson, I. E., Day, J. C. C. & Stone, N. Developing fibre optic Raman probes for
842   applications in clinical spectroscopy. *Chem. Soc. Rev.* **45**, 1919–1934 (2016).

843 31. McGee, R., Blanco, A., Presly, O., Stokes, R. J. & Robert J. Stokes, Ana Blanco, Rachel McGee, O. P.
844   Portable Spatially Offset Raman Spectroscopy for Rapid Hazardous Materials Detection Within Sealed
845   Containers. *Spectroscopy* **33**, 24–30 (2018).

846 32. Matousek, P., Towrie, M. & Parker, A. W. Fluorescence background suppression in Raman
847   spectroscopy using combined Kerr gated and shifted excitation Raman difference techniques. *J. Raman
848   Spectrosc.* **33**, 238–242 (2002).

849 33. Cebeci-Maltaş, D., Wang, P., Alam, M. A., Pinal, R. & Ben-Amotz, D. Photobleaching profile of Raman
850   peaks and fluorescence background. *Eur. Pharm. Rev.* **22**, 18–21 (2017).

851 34. Ghirardello, M. *et al.* Time-Resolved Photoluminescence Microscopy Combined with X-ray Analyses
852   and Raman Spectroscopy Sheds Light on the Imperfect Synthesis of Historical Cadmium Pigments.
853   *Anal. Chem.* **90**, 10771–10779 (2018).

854 35. Afseth, N. K., Bloomfield, M., Wold, J. P. & Matousek, P. A Novel Approach for Subsurface Through-Skin
855   Analysis of Salmon Using Spatially Offset Raman Spectroscopy (SORS). *Appl. Spectrosc.* **68**, 255–262
856   (2014).

857 36. Conti, C., Colombo, C., Realini, M. & Matousek, P. Subsurface analysis of painted sculptures and

858 plasters using micrometre-scale spatially offset Raman spectroscopy (micro-SORS). *J. Raman Spectrosc.*
859 **46**, 476–482 (2015).

860 37. Conti, C. *et al.* Noninvasive Analysis of Thin Turbid Layers Using Microscale Spatially Offset Raman
861 Spectroscopy. *Anal. Chem.* **87**, 5810–5815 (2015).

862 38. American National Standard Institute. American National Standard for Safe Use of Lasers (ANSI Z136.1-
863 2014). *Am. Natl. Stand. Institute,* **IEC**, 60825:2020 (2014).

864 39. Born, M. & Wolf, E. *Principles of Optics*. (Cambridge University Press, 2005).

865 40. Matousek, P. *et al.* Noninvasive Raman Spectroscopy of Human Tissue in vivo. *Appl. Spectrosc.* **60**,
866 758–763 (2006).

867 41. Ghita, A., Matousek, P. & Stone, N. High sensitivity non-invasive detection of calcifications deep inside
868 biological tissue using Transmission Raman Spectroscopy. *J. Biophotonics* **11**, e201600260 (2018).

869 42. Mosca, S. *et al.* Spatially Offset and Transmission Raman Spectroscopy for Determination of Depth of
870 Inclusion in Turbid Matrix. *Anal. Chem.* **91**, 8994–9000 (2019).

871 43. Esmonde-White, F. W. L., Esmonde-White, K. A. & Morris, M. D. Minor Distortions with Major
872 Consequences: Correcting Distortions in Imaging Spectrographs. *Appl. Spectrosc.* **65**, 85–98 (2011).

873 44. Thomas, G. *et al.* Evaluating feasibility of an automated 3-dimensional scanner using Raman
874 spectroscopy for intraoperative breast margin assessment. *Sci. Rep.* **7**, 1–14 (2017).

875 45. Qin, J. *et al.* A line-scan hyperspectral Raman system for spatially offset Raman spectroscopy. *J. Raman*
876 *Spectrosc.* **47**, 437–443 (2016).

877 46. Olds, W. J. *et al.* Spatially offset Raman spectroscopy (SORS) for the analysis and detection of packaged
878 pharmaceuticals and concealed drugs. *Forensic Sci. Int.* **212**, 69–77 (2011).

879 47. Maher, J. R. & Berger, A. J. Determination of Ideal Offset for Spatially Offset Raman Spectroscopy.
880 *Appl. Spectrosc.* **64**, 61–65 (2010).

881 48. Ghita, A., Matousek, P. & Stone, N. Sensitivity of Transmission Raman Spectroscopy Signals to
882 Temperature of Biological Tissues. *Sci. Rep.* **8**, 1–7 (2018).

883 49. Hossain, M. N., Igne, B., Anderson, C. A. & Drennen, J. K. Influence of moisture variation on the
884 performance of Raman spectroscopy in quantitative pharmaceutical analyses. *J. Pharm. Biomed. Anal.*
885 **164**, 528–535 (2019).

886 50. Mestari, A., Gaufrès, R. & Huguet, P. Behaviour of the calibration of a Raman spectrometer with
887 temperature changes. *J. Raman Spectrosc.* **28**, 785–789 (1997).

888 51. E1840-96(2014), A. Standard Guide for Raman Shift Standards for Spectrometer Calibration, ASTM
889 International,tle. *West Conshohocken, PA, 2014* www.astm.org.

890 52. National Institute for Nanotechnology. Standard Spectra.
891 https://www.chem.ualberta.ca/~mccreery/ramanmaterials.html.

892 53. Renishaw. Raman spectroscopy: important considerations. https://www.renishaw.com/en/raman-
893 spectroscopy-important-considerations--25804.

894 54. Allen, M. W. & Mattley, Y. Innovative Raman Sampling. New technique addresses challenges
895 associated with explosives and other sensitive samples. *Optik&Photonik* **4**, 44–47 (2013).

896   55.   Bloomfield, M. *et al.* Non-invasive identification of incoming raw pharmaceutical materials using

897   Spatially Offset Raman Spectroscopy. *J. Pharm. Biomed. Anal.* **76**, 65–69 (2013).

898   56.   Matousek, P. Inverse spatially offset Raman spectroscopy for deep spectroscopy of turbid media. *Appl.*

899   *Spectrosc.* **60**, 1341–1347 (2006).

900   57.   Keller, M. D. *et al.* Development of a spatially offset Raman spectroscopy probe for breast tumor

901   surgical margin evaluation. *J. Biomed. Opt.* **16**, 077006 (2011).

902   58.   Ma, J. & Ben-Amotz, D. Rapid Micro-Raman Imaging Using Fiber-Bundle Image Compression. *Appl.*

903   *Spectrosc.* **51**, 1845–1848 (1997).

904   59.   Liao, Z., Sinjab, F., Gibson, G., Padgett, M. & Notingher, I. DMD-based software-configurable spatially-

905   offset Raman spectroscopy for spectral depth-profiling of optically turbid samples. *Opt. Express* **24**,

906   12701 (2016).

907   60.   Schulmerich, M. V., Dooley, K. A., Morris, M. D., Vanasse, T. M. & Goldstein, S. A. Transcutaneous fiber

908   optic Raman spectroscopy of bone using annular illumination and a circular array of collection fibers. *J.*

909   *Biomed. Opt.* **11**, 060502 (2006).

910   61.   Eliasson, C., Claybourn, M. & Matousek, P. Deep subsurface Raman spectroscopy of turbid media by a

911   defocused collection system. *Appl Spectrosc* **61**, 1123–1127 (2007).

912   62.   Conti, C., Realini, M., Colombo, C. & Matousek, P. Comparison of key modalities of micro-scale spatially

913   offset Raman spectroscopy. *Analyst* **140**, 8127–8133 (2015).

914   63.   Schrader, B. & Bergmann, G. Die Intensität des Ramanspektrums polykristalliner Substanzen. *Anal.*

915   *Chemie* **225**, 230–247 (1967).

916   64.   Matousek, P. & Parker, A. W. Bulk Raman Analysis of Pharmaceutical Tablets. *Appl. Spectrosc.* **60**,

917   1353–1357 (2006). **The first demonstration of transmission Raman spectroscopy (TRS) volumetric**

918   **sensing capability.**

919   65.   Stone, N., Faulds, K., Graham, D. & Matousek, P. Prospects of deep Raman spectroscopy for

920   noninvasive detection of conjugated surface enhanced resonance Raman scattering nanoparticles

921   buried within 25 mm of mammalian tissue. *Anal. Chem.* **82**, 3969–3973 (2010). **The first conceptual**

922   **demonstration of surface-enhanced spatially offset Raman spectroscopy (SESORS).**

923   66.   Stone, N. *et al.* Surface enhanced spatially offset Raman spectroscopic (SESORS) imaging – the next

924   dimension. *Chem. Sci.* **2**, 776 (2011). **The first demonstration of surface-enhanced spatially offset**

925   **Raman spectroscopy (SESORS) imaging.**

926   67.   Sharma, B., Frontiera, R. R., Henry, A., Ringe, E. & Duyne, R. P. Van. SERS : Materials , applications , and

927   the future Surface enhanced Raman spectroscopy (SERS) is a powerful vibrational. *Mater. Today* **15**,

928   16–25 (2012).

929   68.   Jeanmaire, D. L. & Van Duyne, R. P. Surface raman spectroelectrochemistry. Part I. Heterocyclic,

930   aromatic, and aliphatic amines adsorbed on the anodized silver electrode. *J. Electroanal. Chem.* **84**, 1–

931   20 (1977).

932   69.   Hao, E. & Schatz, G. C. Electromagnetic fields around silver nanoparticles and dimers. *J. Chem. Phys.*

933   **120**, 357–366 (2004).

934   70.   Qian, X. *et al.* In vivo tumor targeting and spectroscopic detection with surface-enhanced Raman
935   nanoparticle tags. *Nat. Biotechnol.* **26**, 83 (2007).

936   71.   Moore, T. J. *et al.* In vitro and in vivo sers biosensing for disease diagnosis. *Biosensors* **8**, (2018).

937   72.   Schlücker, S. Surface-Enhanced Raman Spectroscopy: Concepts and Chemical Applications. *Angew.*
938   *Chemie Int. Ed.* **53**, 4756–4795 (2014).

939   73.   Gardner, B., Stone, N. & Matousek, P. Noninvasive simultaneous monitoring of pH and depth using
940   surface-enhanced deep Raman spectroscopy. *J. Raman Spectrosc.* **51**, 1078–1082 (2020). **The first**
941   **conceptual demonstration of surface-enhanced spatially offset Raman spectroscopy (SESORS) to**
942   **measure pH**

943   74.   Laing, S., Gracie, K. & Faulds, K. Multiplex in vitro detection using SERS. *Chem. Soc. Rev.* **45**, 1901–1918
944   (2016).

945   75.   Conti, C., Colombo, C., Realini, M., Zerbi, G. & Matousek, P. Subsurface Raman Analysis of Thin Painted
946   Layers. *Appl. Spectrosc.* **68**, 686–691 (2014). **The first conceptual demonstration of micro-SORS, a**
947   **high-resolution variant of spatially offset Raman spectroscopy.**

948   76.   Matousek, P., Conti, C., Realini, M. & Colombo, C. Micro-scale spatially offset Raman spectroscopy for
949   non-invasive subsurface analysis of turbid materials. *Analyst* **141**, 731–739 (2016).

950   77.   Buckley, K. *et al.* Non-invasive spectroscopy of transfusable red blood cells stored inside sealed plastic
951   blood-bags. *Analyst* **141**, 1678–1685 (2016).

952   78.   Di, Z. *et al.* Spatially offset Raman microspectroscopy of highly scattering tissue: theory and
953   experiment. *J. Mod. Opt.* **62**, 97–101 (2015).

954   79.   Conti, C. & others. Analytical Capability of Defocused μ-SORS in the Chemical Interrogation of Thin
955   Turbid Painted Layers. *Appl Spectrosc.* **70**, 156–161 (2016).

956   80.   Gardner, B., Stone, N. & Matousek, P. Noninvasive Determination of Depth in Transmission Raman
957   Spectroscopy in Turbid Media Based on Sample Differential Transmittance. *Anal. Chem.* **89**, 9730–9733
958   (2017).

959   81.   Agilent. Resolve Handheld Raman Analyzer for Through-Barrier Chemical Identificationle.
960   https://www.agilent.com/en/product/molecular-spectroscopy/raman-spectroscopy/handheld-raman-
961   chemical-detection-systems/resolve-handheld-raman-analyzer-for-through-barrier-chemical-
962   identification.

963   82.   Agilent. Cobalt Insight200M - The Bottle Screener for Liquid, Aerosols & Gels.
964   https://www.agilent.com/en/product/molecular-spectroscopy/raman-spectroscopy/raman-aviation-
965   security-systems/cobalt-insight200m-the-bottle-screener-for-liquid-aerosols-gels.

966   83.   Microsoft Corporation. Microsoft Excel. https://office.microsoft.com/excel.

967   84.   MATLAB. (R2019b),Eigenvector Research,The MathWorks Inc., Natick, Massachusetts.
968   https://www.mathworks.com/products/matlab.html (2018).

969   85.   Widjaja, E. *et al.* Band-target entropy minimization (BTEM) applied to hyperspectral Raman image
970   data. *Appl Spectrosc.* **57**, 1353–1362 (2003).

971   86.   Churchwell, J. H. *et al.* Adaptive band target entropy minimization: Optimization for the decomposition

972   of spatially offset Raman spectra of bone. *J Raman Spectrosc.* **51**, 66–78 (2020).

973   87.   Chen, K., Massie, C. & Berger, A. J. Soft-tissue spectral subtraction improves transcutaneous Raman

974   estimates of murine bone strength in vivo. *J. Biophotonics* **13**, 1–11 (2020).

975   88.   Matousek, P. *et al.* Numerical Simulations of Subsurface Probing in Diffusely Scattering Media Using

976   Spatially Offset Raman Spectroscopy. *Appl. Spectrosc.* **59**, 1485–1492 (2005).

977   89.   Keller, M. D., Wilson, R. H., Mycek, M.-A. & Mahadevan-Jansen, A. Monte Carlo Model of Spatially

978   Offset Raman Spectroscopy for Breast Tumor Margin Analysis. *Appl. Spectrosc.* **64**, 607–614 (2010).

979   90.   OriginLab. v2019b, Northampton, MA, USA. https://www.originlab.com/ (2019).

980   91.   GRAMS/AI. Thermo Scientific, USA. https://www.thermofisher.com/order/catalog/product/INF-

981   15000#/INF-15000.

982   92.   Rencher, A. C. Methods of multivariate analysis. *Choice Rev. Online* **33**, 33-1586-33–1586 (1995).

983   93.   SOLO. Eigenvector Research,Manson, WA USA. https://eigenvector.com/software/solo/.

984   94.   Wiley Science Solution. KnowItALL Raman Spectral Database Collection.

985   https://sciencesolutions.wiley.com/solutions/technique/raman/knowitall-raman-collection/.

986   95.   Gmbh s.t.japan Europe. spectral database. https://katja-hm.jimdofree.com/spectra-databases-1/.

987   96.   RRUFF. Raman and XRF free database. https://rruff.info/.

988   97.   HORIBA. Raman Spectral Libraries. https://www.horiba.com/uk/scientific/products/raman-

989   spectroscopy/accessories/raman-spectral-libraries/.

990   98.   ThermoFisher Scientific. Raman Libraries and Software.

991   https://www.thermofisher.com/search/browse/featured/uk/en/80013171/Raman+Libraries+And+Soft

992   ware.

993   99.   OPUS. Bruker Optik GmbH, Germany. https://www.bruker.com/products/infrared-near-infrared-and-

994   raman-spectroscopy/opus-spectroscopy-software.html.

995   100.   Frisch, M. J. *et al.* Gaussiann 09. Gaussian 09, Revision B.01, Gaussian, Inc., (2009).

996   101.   Griffen, J. A., Owen, A. W., Burley, J., Taresco, V. & Matousek, P. Rapid quantification of low level

997   polymorph content in a solid dose form using transmission Raman spectroscopy. *J. Pharm. Biomed.*

998   *Anal.* **128**, 35–45 (2016).

999   102.   WiRE TM. Renishaw, United Kingdom. https://www.renishaw.com/en/renishaw-enhancing-efficiency-

1000   in-manufacturing-and-healthcare--

1001   45346?utm_expid=.1bs9dmsBTVCDshRo2EAK8A.1&utm_referrer=https%3A%2F%2Fwww.google.com

1002   %2F.

1003   103.   Crytospec. P. Lasch, Berlin, Germany. http://www.cytospec.com/ftir.php.

1004   104.   Kwang, S. Y. & Frontiera, R. R. Spatially Offset Femtosecond Stimulated Raman Spectroscopy:

1005   Observing Exciton Transport through a Vibrational Lens. *J. Phys. Chem. Lett.* **11**, 4337–4344 (2020).

1006   105.   Samuel, A. Z., Yabumoto, S., Kawamura, K. & Iwata, K. Rapid microstructure characterization of

1007   polymer thin films with 2D-array multifocus Raman microspectroscopy. *Analyst* **140**, 1847–1851

1008   (2015).

1009   106.   Shin, K. & Chung, H. Wide area coverage Raman spectroscopy for reliable quantitative analysis and its

1010   applications. *Analyst* (2013) doi:10.1039/c3an36843b.

1011   107.   Paudel, A., Raijada, D. & Rantanen, J. Raman spectroscopy in pharmaceutical product design. *Adv. Drug*

1012   *Deliv. Rev.* **89**, 3–20 (2015).

1013   108.   Kim, M., Chung, H. & Jung, Y. M. Accurate determination of polyethylene pellet density using

1014   transmission Raman spectroscopy. *J. Raman Spectrosc.* **42**, 1967–1976 (2011).

1015   109.   Hooijschuur, J. H., Iping Petterson, I. E., Davies, G. R., Gooijer, C. & Ariese, F. Time resolved Raman

1016   spectroscopy for depth analysis of multi-layered mineral samples. *J. Raman Spectrosc.* **44**, 1540–1547

1017   (2013).

1018   110.   Verkaaik, M. F. C., Hooijschuur, J. H., Davies, G. R. & Ariese, F. Raman Spectroscopic Techniques for

1019   Planetary Exploration: Detecting Microorganisms through Minerals. *Astrobiology* **15**, 697–707 (2015).

1020   111.   Matthiae, M. & Kristensen, A. Hyperspectral spatially offset Raman spectroscopy in a microfluidic

1021   channel. *Opt. Express* **27**, 3782 (2019).

1022   112.   Loeffen, P. W. *et al.* Spatially offset Raman spectroscopy (SORS) for liquid screening. *Opt. Photonics*

1023   *Counterterrorism Crime Fight. VII; Opt. Mater. Def. Syst. Technol. VIII; Quantum-Physics-based Inf.*

1024   *Secur.* **8189**, 81890C (2011).

1025   113.   Eliasson, C. & Matousek, P. Noninvasive authentication of pharmaceutical products through packaging

1026   using spatially offset Raman spectroscopy, Anal. *Chem* **79**, 1696–1701 (2007).

1027   114.   LaserFocusWorld. RAMAN SPECTROSCOPY: Spatial offset broadens applications for Raman

1028   spectroscopy. https://www.laserfocusworld.com/test-measurement/test-

1029   measurement/article/16552969/raman-spectroscopy-spatial-offset-broadens-applications-for-raman-

1030   spectroscopy (2007).

1031   115.   Johansson, J., Sparen, A., Svensson, O., Folestad, S. & Claybourn, M. Quantitative transmission raman

1032   spectroscopy of pharmaceutical tablets and capsules. *Appl. Spectrosc.* **61**, 1211–1218 (2007).

1033   116.   Matousek, P. & Parker, A. W. Non-invasive probing of pharmaceutical capsules using transmission

1034   Raman spectroscopy. *J. Raman Spectrosc.* **38**, 563–567 (2007).

1035   117.   Agilent. TRS100 Quantitative Pharmaceutical Analysis System.

1036   https://www.agilent.com/en/product/molecular-spectroscopy/raman-spectroscopy/raman-

1037   pharmaceutical-analysis-systems/trs100-quantitative-pharmaceutical-analysis-system.

1038   118.   Griffen, J. A., Owen, A. W., Andrews, D. & Matousek, P. Recent advances in pharmaceutical analysis

1039   using transmission Raman spectroscopy. *Spectroscopy* **32**, 37–43 (2017).

1040   119.   21CFR211.84. CFR - Code of Federal Regulations Title 21.

1041   https://www.accessdata.fda.gov/scripts/cdrh/cfdocs/cfcfr/CFRSearch.cfm?fr=211.84 (2020).

1042   120.   Agilent. RapID Raw Material ID Verification System. https://www.agilent.com/en/product/molecular-

1043   spectroscopy/raman-spectroscopy/raman-pharmaceutical-analysis-systems/rapid-raw-material-id-

1044   verification-system.

1045   121.   Agilent. Vaya Handheld Raman Spectrometer for Raw Material Identification.

1046   https://www.agilent.com/en/product/molecular-spectroscopy/raman-spectroscopy/raman-

1047   pharmaceutical-analysis-systems/vaya-handheld-raman-spectrometer-for-raw-material-identification.

1048   122.   Aina, A., Hargreaves, M. D., Matousek, P. & Burley, J. C. Transmission Raman spectroscopy as a tool for
1049   quantifying polymorphic content of pharmaceutical formulations. *Analyst* **135**, 2328 (2010).

1050   123.   Song, S. W. *et al.* Hyperspectral Raman Line Mapping as an Effective Tool To Monitor the Coating
1051   Thickness of Pharmaceutical Tablets. *Anal. Chem.* **91**, 5810–5816 (2019).

1052   124.   Eliasson, C., Macleod, N. A. & Matousek, P. Noninvasive Detection of Concealed Liquid Explosives Using
1053   Raman Spectroscopy. *Anal. Chem.* **79**, 8185–8189 (2007).

1054   125.   Stokes, R. J. *et al.* New capability for hazardous materials ID within sealed containers using a portable
1055   spatially offset Raman spectroscopy (SORS) device. in *Proc. SPIE 9995 999506* (2016).

1056   126.   Zachhuber, B., Gasser, C., Chrysostom, E. T. H. & Lendl, B. Stand-off spatial offset Raman spectroscopy
1057   for the detection of concealed content in distant objects,. *Anal Chem* **83**, 9424–9438 (2011).

1058   127.   Cletus, B. *et al.* Combined time- and space-resolved Raman spectrometer for the non-invasive depth
1059   profiling of chemical hazards. *Anal Bioanal Chem* **403**, 255–263 (2012).

1060   128.   R. J. Hopkins, S. H. P. & Shand, N. C. Short-wave infrared excited spatially offset Raman spectroscopy
1061   (SORS) for through-barrier detection. *Analyst* **137**, 4408 (2012).

1062   129.   Lewis, I. R., Daniel, N. W. & Griffiths, P. R. Interpretation of Raman Spectra of Nitro-Containing
1063   Explosive Materials. Part I: Group Frequency and Structural Class Membership. *Appl. Spectrosc.* **51**,
1064   1854–1867 (1997).

1065   130.   Daniel, N. W., Lewis, I. R. & Griffiths, P. R. Interpretation of Raman Spectra of Nitro-Containing
1066   Explosive Materials. Part II: The Implementation of Neural, Fuzzy, and Statistical Models for
1067   Unsupervised Pattern Recognition. *Appl. Spectrosc.* **51**, 1868–1879 (1997).

1068   131.   Schulmerich, M. V *et al.* Transcutaneous Raman spectroscopy of bone tissue using a non-confocalfiber
1069   optic array probe. in *Proc. SPIE 6093 60930O* (2006).

1070   132.   Dooley, M., McLaren, J., Rose, F. R. A. J. & Notingher, I. Investigating the feasibility of spatially offset
1071   Raman spectroscopy for in-vivo monitoring of bone healing in rat calvarial defect models. *J.*
1072   *Biophotonics* **13**, (2020).

1073   133.   Stone, N. & Matousek, P. Advanced transmission Raman spectroscopy: A promising tool for breast
1074   disease diagnosis. *Cancer Res.* **68**, 4424–4430 (2008).

1075   134.   Stone, N., Baker, R., Rogers, K., Parker, A. W. & Matousek, P. Subsurface probing of calcifications with
1076   spatially offset Raman spectroscopy (SORS): Future possibilities for the diagnosis of breast cancer.
1077   *Analyst* **132**, 899–905 (2007).

1078   135.   Gardner, B., Matousek, P. & Stone, N. Subsurface Chemically Specific Measurement of pH Levels in
1079   Biological Tissues Using Combined Surface-Enhanced and Deep Raman. *Anal. Chem.* **91**, 10984–10987
1080   (2019).

1081   136.   Keller, M. D., Majumder, S. K. & Mahadevan-Jansen, A. Spatially offset Raman spectroscopy of layered
1082   soft tissues. *Opt. Lett.* **34**, 926–928 (2009).

1083   137.   Schulmerich, M. V, Finney, W. F., Fredricks, R. A. & Morris, M. D. Subsurface Raman spectroscopy and
1084   mapping using a globally illuminated non confocal fiber optic array probe in the presence of Raman
1085   photon migration,. *Appl Spectrosc.* **60**, 109 (2006).

1086   138.   Schulmerich, M. V *et al.* Noninvasive Raman tomographic imaging of canine bone tissue. *J. Biomed.*
1087   *Opt.* **13**, 020506 (2008).

1088   139.   Srinivasan, S. *et al.* Image-guided Raman spectroscopic recovery ofcanine cortical bone contrast in situ.
1089   *Opt. Express* **16**, 12190 (2008).

1090   140.   Demers, J.-L. H., Esmonde-White, F. W. L., Esmonde-White, K. A., Morris, M. D. & Pogue, B. W. Next-
1091   generation Raman tomography instrument for non-invasive in vivo bone imaging. *Biomed. Opt. Express*
1092   **6**, 793 (2015).

1093   141.   Demers, J.-L., Davis, S., Pogue, B. W. & Morris, M. D. Measurement of Raman Spectra for Tomographic
1094   Reconstruction. *Biomed. Opt. 3-D Imaging* BSu5A.8 (2012) doi:10.1364/BIOMED.2012.BSu5A.8.

1095   142.   Jiang, S., Pogue, B. W., Laughney, A. M., Kogel, C. A. & Paulsen, K. D. Measurement of pressure-
1096   displacement kinetics of hemoglobin in normal breast tissue with near-infrared spectral imaging. *Appl.*
1097   *Opt.* **48**, D130 (2009).

1098   143.   Sil, S. & Umapathy, S. Raman spectroscopy explores molecular structural signatures of hidden
1099   materials in depth: Universal Multiple Angle Raman Spectroscopy. *Sci. Rep.* **4**, 5308 (2015).

1100   144.   Gardner, B., Stone, N. & Matousek, P. Non-invasive chemically specific measurement of subsurface
1101   temperature in biological tissues using surface-enhanced spatially offset Raman spectroscopy. *Faraday*
1102   *Discuss.* **187**, 329–339 (2016)**. The first conceptual demonstration of T-SESORS, a variant of surface-**
1103   **enhanced spatially offset Raman spectroscopy (SESORS) and transmission Raman spectroscopy**
1104   **(TRS).**

1105   145.   Gardner, B., Matousek, P. & Stone, N. Direct monitoring of light mediated hyperthermia induced within
1106   mammalian tissues using surface enhanced spatially offset Raman spectroscopy (T-SESORS). *Analyst*
1107   **144**, 3552–3555 (2019).

1108   146.   Vardaki, M. Z. *et al.* Raman spectroscopy of stored red blood cell concentrate within sealed transfusion
1109   blood bags. *Analyst* **143**, 6006–6013 (2018).

1110   147.   Vardaki, M. Z. & Kourkoumelis, N. Tissue Phantoms for Biomedical Applications in Raman
1111   Spectroscopy: A Review. *Biomed. Eng. Comput. Biol.* **11**, 1–15 (2020).

1112   148.   Nicolson, F. *et al.* Non-invasive In Vivo Imaging of Cancer Using Surface-Enhanced Spatially Offset
1113   Raman Spectroscopy (SESORS). *Theranostics* **9**, 5899–5913 (2019).

1114   149.   Ma, K. *et al.* In vivo, transcutaneous glucose sensing using surface-enhanced spatially offset Raman
1115   spectroscopy: multiple rats, improved hypoglycemic accuracy, low incident power, and continuous
1116   monitoring for greater than 17 days,. *Anal Chem* **83**, 9146–9152 (2011).

1117   150.   Sharma, B., Ma, K., Glucksberg, M. R. & Van Duyne, R. P. Seeing through Bone with Surface-Enhanced
1118   Spatially Offset Raman Spectroscopy. *J. Am. Chem. Soc.* **135**, 17290–17293 (2013).

1119   151.   Moody, A. S., Baghernejad, P. C., Webb, K. R. & Sharma, B. Surface Enhanced Spatially Offset Raman
1120   Spectroscopy Detection of Neurochemicals Through the Skull. *Anal. Chem.* **89**, 5688–5692 (2017).

1121   152.   Moody, A. S., Payne, T. D., Barth, B. A. & Sharma, B. Surface-enhanced spatially-offset Raman
1122   spectroscopy (SESORS) for detection of neurochemicals through the skull at physiologically relevant
1123   concentrations. *Analyst* **145**, 1885–1893 (2020).

1124   153.   Qin, J., Chao, K. & Kim, M. S. Nondestructive evaluation of internal maturity of tomatoes using spatially
1125   offset Raman spectroscopy,. *Postharvest Biol Technol.* **71**, 21–31 (2012).

1126   154.   Morey, R. *et al.* Non-invasive identification of potato varieties and prediction of the origin of tuber
1127   cultivation using spatially offset Raman spectroscopy. *Anal. Bioanal. Chem.* **412**, 4585–4594 (2020).

1128   155.   Ellis, D. I. *et al.* Through-container, extremely low concentration detection of multiple chemical
1129   markers of counterfeit alcohol using a handheld SORS device,. *Sci Re* **7**, 12082 (2017).

1130   156.   Conti, C. *et al.* Advances in Raman spectroscopy for the non-destructive subsurface analysis of
1131   artworks: Micro-SORS. *J. Cult. Herit.* **43**, 319–328 (2020).

1132   157.   Botteon, A. *et al.* Non-invasive characterisation of molecular diffusion of agent into turbid matrix using
1133   micro-SORS. *Talanta* **218**, 121078 (2020).

1134   158.   Janssens, K., Dik, J., Cotte, M. & Susini, J. Photon-based techniques for nondestructive subsurface
1135   analysis of painted cultural heritage artifacts. *Acc. Chem. Res.* **43**, 814–825 (2010).

1136   159.   Tournié, A. *et al.* Ancient Greek text concealed on the back of unrolled papyrus revealed through
1137   shortwave-infrared hyperspectral imaging. *Sci. Adv.* **5**, 1–9 (2019).

1138   160.   Brunetti, B. *et al.* Non-invasive investigations of paintings by portable instrumentation: The MOLAB
1139   experience. *Top. Curr. Chem.* **374**, 1–35 (2016).

1140   161.   Realini, M., Conti, C., Botteon, A., Colombo, C. & Matousek, P. Development of a full micro-scale
1141   spatially offset Raman spectroscopy prototype as a portable analytical tool. *Analyst* **142**, 351–355
1142   (2017).

1143   162.   Botteon, A. *et al.* Non-invasive and in situ investigation of layers sequence in panel paintings by
1144   portable micro-spatially offset Raman spectroscopy. *J. Raman Spectrosc.* **51**, 2016–2021 (2020).

1145   163.   Casadio, F., Daher, C. & Bellot-Gurlet, L. Raman Spectroscopy of cultural heritage Materials: Overview
1146   of Applications and New Frontiers in Instrumentation, Sampling Modalities, and Data Processing. *Top.*
1147   *Curr. Chem.* **374**, 62 (2016).

1148   164.   Stone, N., Kendall, C. & Barr, H. Raman Spectroscopy as a Potential Tool for Early Diagnosis of
1149   Malignancies in Esophageal and Bladder Tissues. in *Handbook of Vibrational Spectroscopy* (ed. Diem,
1150   M.) (John Wiley & Sons, Ltd, 2008). doi:10.1002/0470027320.s8931.

1151   165.   Isabelle, M. *et al.* Multi-centre Raman spectral mapping of oesophageal cancer tissues: A study to
1152   assess system transferability. *Faraday Discuss.* **187**, 87–103 (2016).

1153   166.   ChemSpider. Raman Spectra database. *royal society of chemistry*
1154   http://www.chemspider.com/Spectra.aspx?st=R.

1155   167.   Harvey, C. E. *et al.* Looking inside catalyst extrudates with time-resolved surface-enhanced Raman
1156   spectroscopy (TR-SERS). *Appl. Spectrosc.* **66**, 1179–1185 (2012).

1157   168.   Corden, C., Matousek, P., Conti, C. & Notingher, I. Sub-Surface Molecular Analysis and Imaging in
1158   Turbid Media Using Time-Gated Raman Spectral Multiplexing. *Appl. Spectrosc.* 000370282094605
1159   (2020) doi:10.1177/0003702820946054.

1160   169.   Kekkonen, J., Nissinen, J. & Nissinen, I. Depth Analysis of Semi-Transparent Media by a Time-Correlated
1161   CMOS SPAD Line Sensor-Based Depth-Resolving Raman Spectrometer. *IEEE Sens. J.* **19**, 6711–6720

1162   (2019).

1163   170.   Mosca, S. *et al.* Spatially Offset Raman Spectroscopy - How Deep? *"in Prep.* (2021).

1164   171.   Bersani, D., Conti, C., Matousek, P., Pozzi, F. & Vandenabeele, P. Methodological evolutions of Raman

1165   spectroscopy in art and archaeology. *Anal. Methods* **8**, 8395–8409 (2016).

1166   172.   Conti, C., Botteon, A., Colombo, C., Realini, M. & Matousek, P. Investigation of Heterogeneous Painted

1167   Systems by Micro-Spatially Offset Raman Spectroscopy. *Anal. Chem.* **89**, 11476–11483 (2017).

1168   173.   Botteon, A. *et al.* Exploring street art paintings by microspatially offset Raman spectroscopy. *J. Raman*

1169   *Spectrosc.* **49**, 1652–1659 (2018).

1170   174.   Barnett, P. D. & Angel, S. M. Miniature Spatial Heterodyne Raman Spectrometer with a Cell Phone

1171   Camera Detector. *Appl. Spectrosc.* **71**, 988–995 (2017).

1172   175.   Agilent. Raman Spectroscopy - Innovative Raman Technology for Noninvasive Through-Barrier

1173   Chemical Analysis. https://www.agilent.com/en/product/molecular-spectroscopy/raman-spectroscopy

1174   (2020).

1175   176.   Loeffen, P. W. *et al.* The performance of spatially offset Raman spectroscopy for liquid explosive

1176   detection. in *Optics and Photonics for Counterterrorism, Crime Fighting, and Defence XII* (eds. Burgess,

1177   D. et al.) 12 (SPIE, 2016). doi:10.1117/12.2241535.

1178   177.   American Pharmaceutical Review. Transmission Raman Spectroscopy for Pharmaceutical Analysis.

1179   https://www.americanpharmaceuticalreview.com/Featured-Articles/358425-Transmission-Raman-

1180   Spectroscopy-for-Pharmaceutical-Analysis/ (2019).

1181   178.   Waldron, A., Allen, A., Colón, A., Carter, J. C. & Angel, S. M. A Monolithic Spatial Heterodyne Raman

1182   Spectrometer: Initial Tests. *Appl. Spectrosc.* **75**, 57–69 (2021).

1183   179.   Griffen, J. A., Owen, A. W. & Matousek, P. Development of Transmission Raman Spectroscopy towards

1184   the in line, high throughput and non-destructive quantitative analysis of pharmaceutical solid oral

1185   dose. *Analyst* **140**, 107–112 (2015).

1186   180.   Loeffen, P. W. *et al.* Chemical and explosives point detection through opaque containers using spatially

1187   offset Raman spectroscopy (SORS). *Chem. Biol. Radiol. Nucl. Explos. Sens. XII* **8018**, 80181E (2011).

1188   181.   Thomas, K. J., Sheeba, M., Nampoori, V. P. N., Vallabhan, C. P. G. & Radhakrishnan, P. Raman spectra of

1189   polymethyl methacrylate optical fibres excited by a 532 nm diode pumped solid state laser. *J. Opt. A*

1190   *Pure Appl. Opt.* **10**, 1–6 (2008).

1191

Highlighted references

13.   Matousek, P. et al. Subsurface probing in diffusely scattering media using spatially offset Raman spectroscopy. *Appl. Spectrosc.* **59**, 393–400 (2005). **The first conceptual demonstration of spatially offset Raman spectroscopy (SORS).**

64.   Matousek, P. & Parker, A. W. Bulk Raman analysis of pharmaceutical tablets. *Appl. Spectrosc.* **60**, 1353–1357 (2006). **The first demonstration of transmission Raman spectroscopy (TRS) volumetric sensing capability.**

65.   Stone, N., Faulds, K., Graham, D. & Matousek, P. Prospects of deep Raman spectroscopy for noninvasive detection of conjugated surface enhanced resonance Raman scattering nanoparticles buried within 25 mm of mammalian tissue. *Anal. Chem.* **82**, 3969–3973 (2010). **The first conceptual demonstration of surface-enhanced spatially offset Raman spectroscopy (SESORS).**

66.   Stone, N. et al. Surface enhanced spatially offset Raman spectroscopic (SESORS) imaging - the next dimension. *Chem. Sci.* **2**, 776–780 (2011). **The first demonstration of surface-enhanced spatially offset Raman spectroscopy (SESORS) imaging.**

73.   Gardner, B., Stone, N. & Matousek, P. Non-invasive simultaneous monitoring of pH and depth using surface-enhanced deep Raman spectroscopy. *J. Raman Spectrosc.* **51**, 1078–1082 (2020). **The first conceptual demonstration of surface-enhanced spatially offset Raman spectroscopy (SESORS) to measure pH.**

75.   Conti, C., Colombo, C., Realini, M., Zerbi, G. & Matousek, P. Subsurface Raman analysis of thin painted layers. Appl Spectrosc **68**, 686–691 (2014). **The first conceptual demonstration of micro-SORS, a high-resolution variant of spatially offset Raman spectroscopy.**

144.   Gardner, B., Stone, N. & Matousek, P. Non-invasive chemically specific measurement of subsurface temperature in biological tissues using surface-enhanced spatially offset Raman spectroscopy. *Faraday Discussions* **187**, 329–339 (2016). **The first conceptual demonstration of T-SESORS, a variant of surface-enhanced spatially offset Raman spectroscopy (SESORS) and transmission Raman spectroscopy (TRS).**

1229

1230

1234

1235

1236 **Figure legends**
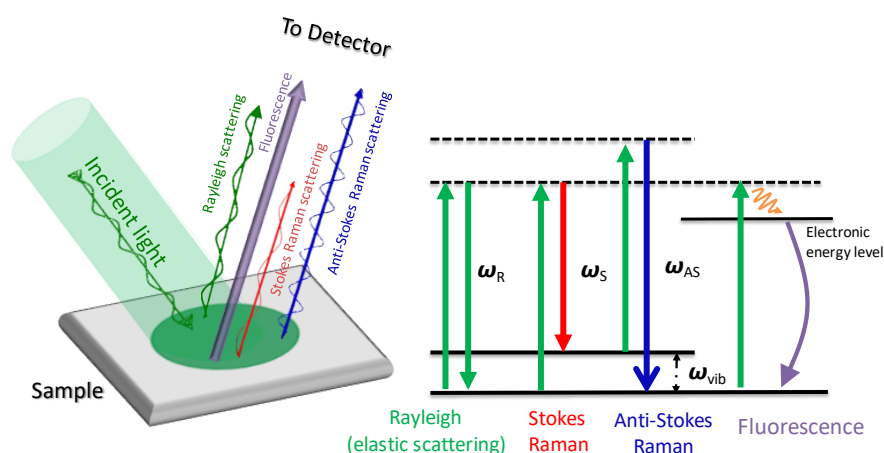
1237

1238 **Fig. 1: Raman scattering.**

1239 When light illuminates a sample, it can interact with the constituent molecules in a number of ways.

1240 Some light may be reflected from the surface through direct specular reflection or undergo elastic

1241 scattering (Rayleigh scattering), resulting in the emission of light from the sample of the same

1242 wavelength as the incident light. If the energy of the illuminating photons matches an electronic

1243 energy level of the molecule, they can excite the molecule to this state and de-excitation subsequently

1244 occurs through the emission of a photon of a longer wavelength than the incident photon

1245 (fluorescence). Raman inelastic scattering can take place where incident photons induce a vibrational

1246 oscillation in the molecule, specific to the chemical moiety[1]. In the case of Stokes scattering, energy is

1247 absorbed by the molecule and the wavelength of the emitted photon is less than that of the incidence

1248 photon. If the molecule is initially in a vibrationally-excited state it can de-excite vibrationally,

1249 transferring energy to the scattered photon (anti-Stokes scattering). All of these interactions can be

1250   measured and give information about the composition and environment of the molecules of interest

1251   in a sample. E_R, energy of Rayleigh scattered photon; E_S, energy of Stokes photon; E_{AS}, energy of anti-

1252   Stokes photon; E_{vib}, vibrational energy level difference of molecule.

1253

1254

1255
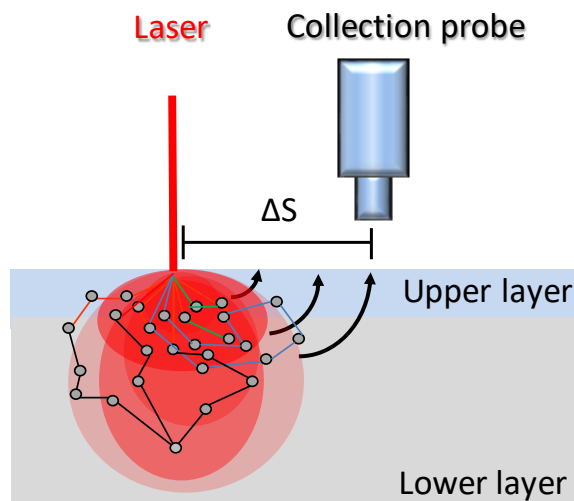
1256

Fig. 2: The SORS concept.

Conventional Raman spectroscopy is ineffective at probing diffusely scattering samples at depth, where photon directions are scrambled and direct imaging cannot be used in a simple way to discriminate between different layers. The diffusive nature of samples leads to a large diffusion of photons sideways, leading to photon spread in all spatial dimensions. In order to detect Raman signals from a deep layer, laser photons first have to penetrate to this layer and get converted into a Raman photon, which must then diffuse back to the surface in order to be detected. Their long 'zig-zag' path leads to a larger sideways spread for photons originating from deeper layers compared to those coming from near the surface. The detection of signals at spatially offset locations (Δs) can therefore detect more of the deeper propagating photons generated in the lower layer than when collecting directly from the illumination point.

1268

1269
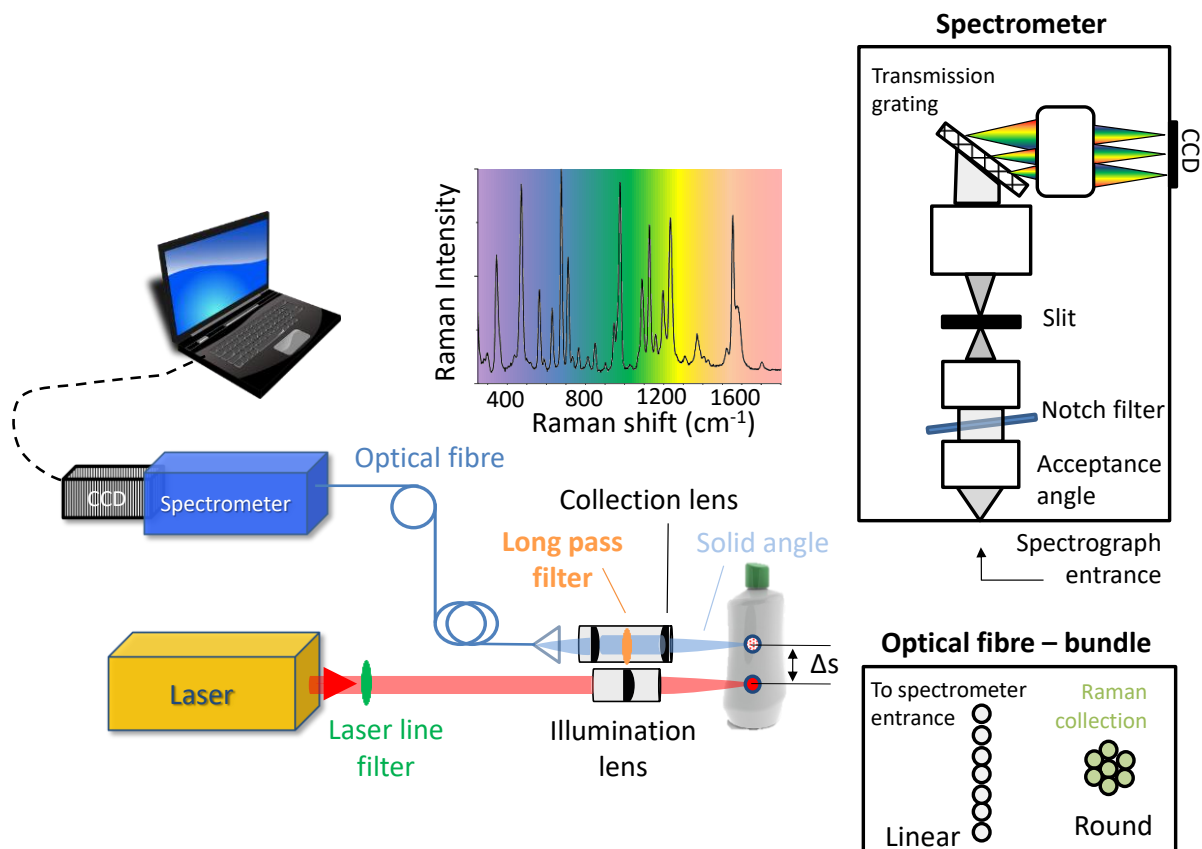
1270

Fig. 3: Schematic diagram of the SORS instrumental setup.

A) In a basic SORS setup, a laser beam — appropriately filtered with a laser line filter to remove extra spectral component — illuminates a sample at a specific point and a SORS signal is collected using a collection lens from a spatially separated location (Δs) on the sample surface. The collected light is filtered using a long-pass filter to eliminate the laser light and then typically transferred into an optical fibre and delivered to a spectrometer. B) Often, round-to-linear optical fibre bundles are used for effectively delivering the collected Raman photons to the spectrometer. The bundle contains several optical fibres in a circular layout at the collection terminal and these are relayed and repositioned into a line configuration at the spectrograph end, matching the shape of spectrograph entrance slit. C) The light is dispersed spectrally inside the spectrograph using a transmission grating and imaged onto a charge-coupled device (CCD). The notch filter transmits Raman radiation and blocks residual laser light. The acceptance angle is the maximum solid angle from which light can be coupled into spectrometer.

1284

1285

1286

1287
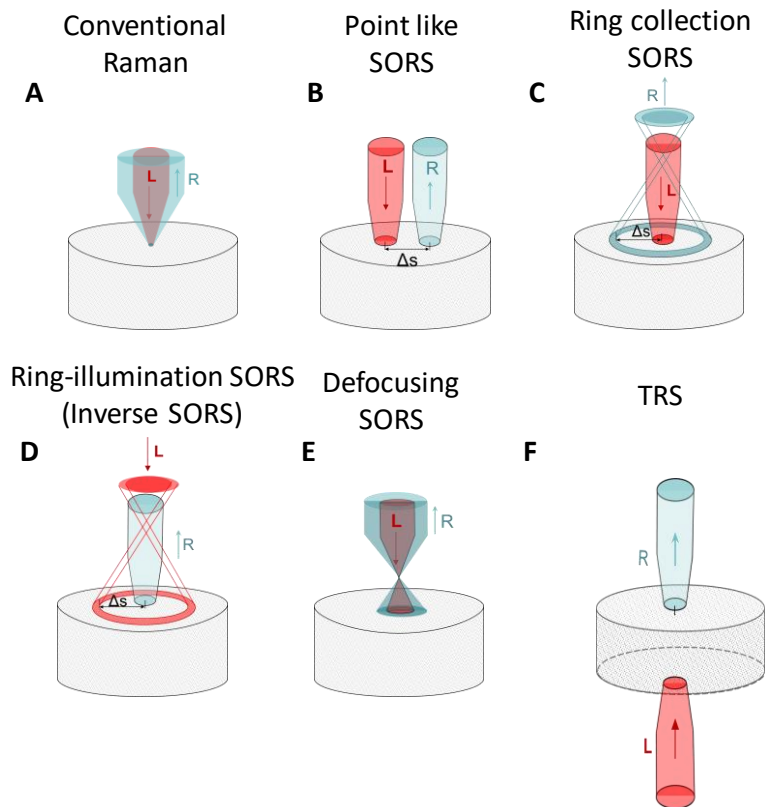
Fig. 4: Variants of spatially offset Raman spectroscopy

A) In conventional Raman spectroscopy, Raman signal is collected from the laser illumination zone. **B)** Point-like spatially offset Raman spectroscopy (SORS) uses near-point illumination and collection areas that are mutually displaced by a spatial offset, Δs. **C)** Ring collection SORS uses a point-like illumination geometry with Raman signal collected through a ring. **D)** Ring illumination SORS, or inverse SORS, uses a ringed illumination zone, with Raman signal collected through a point-like zone at the centre of the ring. **E)** In defocusing SORS, illumination and collection areas remain largely overlapped and their size is controlled by moving the sample relative to the collection optics. Note that this concept does not require for the laser beam to under-fill the microscope objective; the concept works even when these areas are of identical dimensions upon defocusing due to the presence of mutually separated incidence and collection points on the sample surface. **F)** In transmission Raman spectroscopy (TRS), the illumination and collection zones are on the opposite sides of the sample. In all configurations, illumination and collection beams are labelled as L (laser) and R (Raman), respectively.
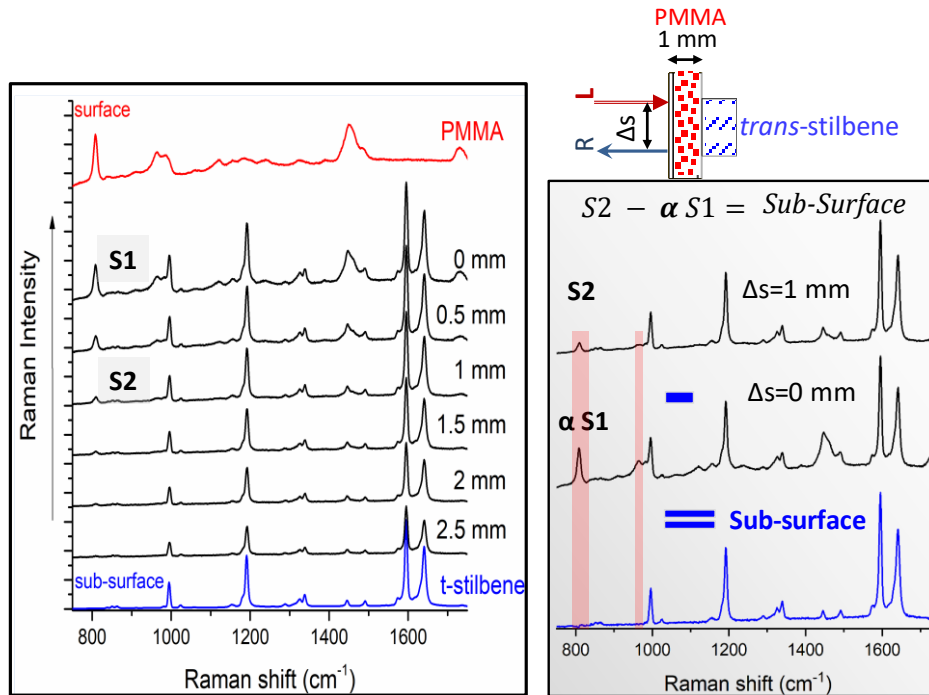
Fig. 5: Representative SORS spectra from a two-layer system. SORS spectra collected at different spatial offset (Δs) from a two-layer system consisting of a 1 mm-thick layer of 20 μm-diameter spheres of poly(methyl methacrylate) (PMMA), over a 2 mm-thick sub-layer of *trans*-stilbene powder. **A)** Raman spectra recovered from a range of different spatial offsets. The spectra are vertically offset for clarity. The top and bottom spectra (red and blue line) are the reference spectra of the surface PMMA and sub-surface *trans*-stilbene layers, respectively. **B)** Schematic of the experimental setup. Trans-stilbene was chosen for the sublayer as it is a particularly strong Raman scatterer. **C)** Illustration of the mathematical process of reconstructing the sub-surface Raman spectrum from the measured SORS spectra. A SORS spectrum collected at a zero spatial offset with a scaling factor α (αS1) is subtracted from a non-zero spatial offset spectrum (S2). The value of α (α = 0.21) was chosen to cancel the presence of Raman contributions from the surface layer; vertical green shading indicates a target band from the surface layer, corresponding to the $v(CH_2)$ vibration modes in PMMA[181], that is eliminated in the subtraction process. An almost-identical spectrum was obtained by performing a band-target entropy minimization (BTEM) multivariate analysis using the entire SORS data set[13]. Adapted with permission from ref.[13], SAGE Publications.
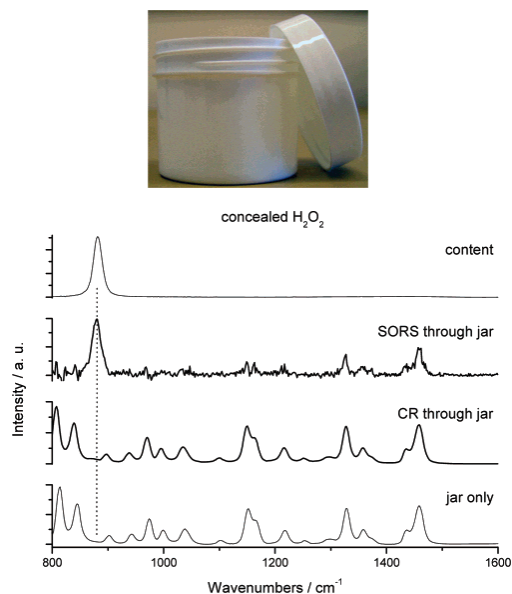
Fig. 6: Analyzing the contents of a plastic container.

Spectra gathered using conventional Raman spectroscopy (CRS) and spatially offset Raman spectroscopy (SORS) through the analysis of a 1.2 mm-thick white plastic jar made of polypropylene, filled with a 30% solution of H_2O_2 in water. The conventional Raman spectrum of the jar containing H_2O_2 (CR through jar) is essentially identical to a reference Raman spectrum of an empty jar (Jar only) with no obvious trace of the Raman signature of H_2O_2 (dashed line). The SORS spectrum of the jar containing H_2O_2 (SORS through jar) shows a strong Raman component that matches the reference spectrum of the aqueous H_2O_2 solution (Content). The residual features in the processed SORS spectrum appearing at the positions corresponding to container Raman bands are caused by imperfect subtraction of the container Raman signal, itself caused by the self-absorption of the spatially offset signal propagating through the probed object. Adapted with permission from ref.[124], ACS.

1338
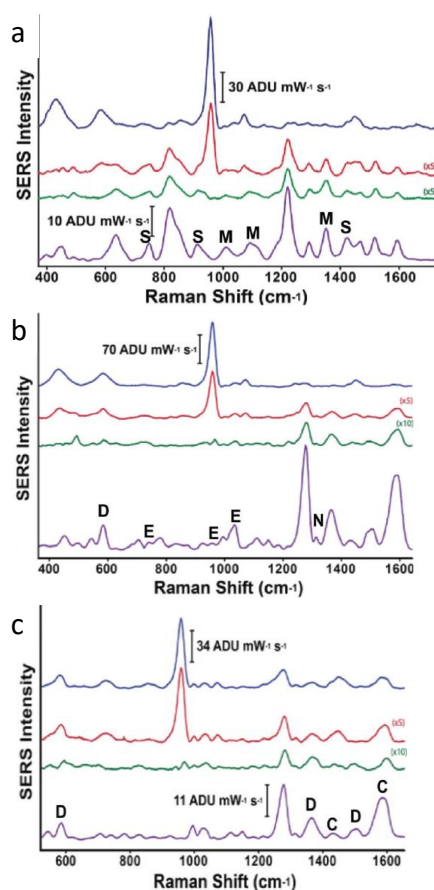
Fig. 7. Analyzing neurotransmitters using surface enhanced spatially offset Raman spectroscopy.
Spectra obtained using surface-enhanced spatially offset Raman spectroscopy (SESORS) of different mixtures of neurotransmitters and gold nanoparticles in an agarose gel, collected through a rat skull. Agarose mixtures containing melatonin and serotonin (A); dopamine, epinephrine and norepinephrine (B) and dopamine and a metabolite of dopamine known as 3,4-dihydroxylphenyl acetic acid (DOPAC) (C) are shown. The top spectrum for each panel represents the contribution from the bone with no spatial offset (blue). The second spectrum (red) is the SESORS spectrum of the neurotransmitters in the agarose gel behind the rat skull with a 2 mm spatial offset. The third spectrum (green) shows a subtraction of the bone spectrum from the SESORS spectrum, revealing a pure spectrum of the neurotransmitter. The bottom spectrum (purple) shows a positive control obtained from directly analysing the neurotransmitters and gold nanoparticles embedded in the agarose gel. Peaks corresponding to specific neutrotransmitters are labelled with upper case letters. S, serotonin; M, melatonin; D, dopamine; E, epinephrine; N, noradrenaline; C, 3,4-dihydroxyphenylacetic acid. Spectra collected with an excitation wavelength of 785 nm, laser power of 90 mW and acquisition time of 120 seconds. Reprinted with permission from ref.[152], RSC.
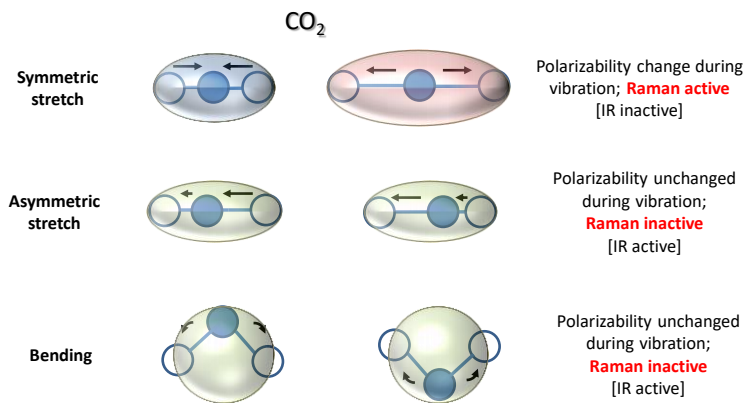
1354

Table 1 Main SORS modalities.

1356

Spatially offset Raman spectroscopy (SORS) modality	Advantages	Disadvantages
Point-like SORS	Simple to implement	High illumination intensities at all spatial offsets
Ring-collection SORS	Effective collection of available Raman signal at the sample surface	High illumination intensities at all spatial offsets
Ring-illumination SORS (inverse SORS)	Enables greater laser powers to be used with larger spatial offsets	Complexity of implementation; moving optical components
Defocusing SORS	Simple to implement	Low layer contrast
Transmission Raman Spectroscopy (TRS)	Volumetric averaging; Suited to overall compositional studies	Does not separate individual layers
Surface enhanced spatially offset Raman spectroscopy (SESORS)	Exceptional sensitivity, high accessible depth and chemical specificity	Requires nanoparticles or surface enhanced Raman spectroscopy (SERS) substrate inside sample
Micro-SORS	High spatial resolution; ideal for thin layers such as paints and coatings	Added complexity as requires a Raman microscope

1357

1358

1359   **Boxes**

1360

CO$_2$

Symmetric stretch — Polarizability change during vibration; **Raman active** [IR inactive]

Asymmetric stretch — Polarizability unchanged during vibration; **Raman inactive** [IR active]

Bending — Polarizability unchanged during vibration; **Raman inactive** [IR active]

1361

1362 **Box 1: Example of Raman-active and infrared-active bond vibrations for CO$_2$**

1363

1364 A CO$_2$ molecule has four fundamental vibrational modes; C-O asymmetric stretching, C-O symmetric

1365 stretching and two O-C-O bending modes that are degenerate (of identical frequencies). Only the

1366 symmetric stretching mode results in a change in polarizability of the molecule and is therefore Raman

1367 active. This mode is unobservable in infrared absorption spectroscopy.

1368

1369

1370

1371 **[H1] Glossary**

1372

1373 **Rayleigh scattering:** The elastic scattering of electromagnetic radiation by particles smaller that the

1374 wavelength of the radiation.

1375

1376 **Polarizability:** The degree to which a molecular dipole changes in response to an external electric field.

1377

1378 **Raman scattering:** The inelastic scattering of photons, where the frequency of the scattered photon

1379 is different from the incident photon.

1380

1381 **Photon shot noise:** Fluctuations of the detected number of photons, caused by the inherent particle-

1382 like properties of photons.

1383

1384   **Lambert's cosine law:** A law describing the cosine dependence of light emission intensity with respect
1385   to the angle of incidence from the surface normal.

1386

1387   **Solid angle:** A measure of the amount of the field of view that an object occupies from a particular
1388   point.
1389

1390   **Acceptance angle:** The maximum incidence angle of an optical ray that is transmitted to the
1391   spectrograph, measured from the optical axis of the spectrograph.

1392

1393   **Cosmic rays:** High energy protons and atomic nuclei that move through space at nearly the speed of
1394   light.

1395

1396   **Surface plasmon resonance:** A resonant oscillation of nanoparticle conduction electrons induced by
1397   incident light; its spectral properties are dependent on nanoparticle size, shape and metal type.

1398

1399   **Monte Carlo simulations:** Numerical algorithms that rely on the random sampling of events.

1400

1401   **Imaging phantoms:** Specially prepared samples that mimic the properties of real biological tissue for
1402   the purposes of optical imaging.

1403

1404   **Polymorphs:** Identical chemicals of different crystalline forms.

1405

1406   **Etaloning:** Wave-like modulation of CCD sensitivity across the sensor caused by light interference and
1407   associated with back-illuminated CCDs.

1408

1409   **Readout noise:** Noise induced by charge digitization circuitry, imprinted on signal when it is read.

1410

1411   **Thermal noise:** Noise induced by thermal fluctuations of charge carriers within a detection element.

1412

1413   **Instrument response function:** In the context of SORS, a combined spectrograph-detector spectral
1414   intensity profile in response to illumination by a spectrally uniform light source.

1415